



HAL
open science

Magnetism of the Acapulco Primitive Achondrite and Implications for the Evolution of Partially Differentiated Bodies

Elias N Mansbach, Benjamin P Weiss, Neesha R Schnepf, Eduardo A Lima, Cauê S Borlina, Nilanjan Chatterjee, Jérôme Gattacceca, Minoru Uehara, Huapei Wang

► To cite this version:

Elias N Mansbach, Benjamin P Weiss, Neesha R Schnepf, Eduardo A Lima, Cauê S Borlina, et al.. Magnetism of the Acapulco Primitive Achondrite and Implications for the Evolution of Partially Differentiated Bodies. *Journal of Geophysical Research. Planets*, 2023, 128 (12), 10.1029/2023je008076 . hal-04346524

HAL Id: hal-04346524

<https://hal.science/hal-04346524>

Submitted on 15 Dec 2023

HAL is a multi-disciplinary open access archive for the deposit and dissemination of scientific research documents, whether they are published or not. The documents may come from teaching and research institutions in France or abroad, or from public or private research centers.

L'archive ouverte pluridisciplinaire **HAL**, est destinée au dépôt et à la diffusion de documents scientifiques de niveau recherche, publiés ou non, émanant des établissements d'enseignement et de recherche français ou étrangers, des laboratoires publics ou privés.



Distributed under a Creative Commons Attribution 4.0 International License

Magnetism of the Acapulco Primitive Achondrite and Implications for the Evolution of Partially Differentiated Bodies



Key Points:

- We studied the rock magnetism properties of the primitive achondrite Acapulco to pave the way for future paleomagnetic investigations
- While bulk samples are poor recorders, silicate grains with metal inclusions may retain stable magnetizations over 4.5 billion years (Ga)
- The presence of tetraenaite means that Acapulco's parent body was likely not catastrophically disrupted at temperatures $>320^{\circ}\text{C}$

Supporting Information:

Supporting Information may be found in the online version of this article.

Correspondence to:

E. N. Mansbach,
mansbach@mit.edu

Citation:

Mansbach, E. N., Weiss, B. P., Schnepf, N. R., Lima, E. A., Borlina, C. S., Chatterjee, N., et al. (2023). Magnetism of the acapulco primitive achondrite and implications for the evolution of partially differentiated bodies. *Journal of Geophysical Research: Planets*, 128, e2023JE008076. <https://doi.org/10.1029/2023JE008076>

Received 29 AUG 2023

Accepted 17 NOV 2023

Author Contributions:

Conceptualization: Elias N. Mansbach, Benjamin P. Weiss

Data curation: Elias N. Mansbach, Benjamin P. Weiss, Neesha R. Schnepf

Formal analysis: Elias N. Mansbach, Benjamin P. Weiss, Neesha R. Schnepf, Eduardo A. Lima, Cauê S. Borlina

Investigation: Elias N. Mansbach, Benjamin P. Weiss, Neesha R. Schnepf, Nilanjan Chatterjee, Jérôme Gattacceca, Minoru Uehara, Huapei Wang

Methodology: Elias N. Mansbach, Benjamin P. Weiss

© 2023. The Authors.

This is an open access article under the terms of the [Creative Commons Attribution License](https://creativecommons.org/licenses/by/4.0/), which permits use, distribution and reproduction in any medium, provided the original work is properly cited.

Elias N. Mansbach¹ , Benjamin P. Weiss¹ , Neesha R. Schnepf² , Eduardo A. Lima¹ , Cauê S. Borlina^{1,3}, Nilanjan Chatterjee¹ , Jérôme Gattacceca⁴ , Minoru Uehara⁴ , and Huapei Wang⁵ 

¹Department of Earth, Atmosphere, and Planetary Sciences, Massachusetts Institute of Technology, Cambridge, MA, USA, ²Laboratory for Atmospheric and Space Physics, University of Colorado, Boulder, CO, USA, ³Department of Earth and Planetary Science, Johns Hopkins University, Baltimore, MD, USA, ⁴CNRS, Aix Marseille Université, IRD, INRAE, CEREGE, Aix-en-Provence, France, ⁵School of Geophysics and Geomatics, China University of Geosciences, Wuhan, China

Abstract Primitive achondrites like the acapulcoites-lodranites (AL) clan are meteorites that formed on bodies in the process of forming a metallic core, providing a unique window into how early solar system processes transformed unmelted material into differentiated bodies. However, the size and structure of the parent body of ALs and other primitive achondrites are largely unknown. Paleomagnetism can establish the presence or absence of a metallic core by looking for evidence of a dynamo field. We conducted a magnetic study of the Acapulco acapulcoite to determine its ferromagnetic minerals and their recording properties. This is the first detailed rock magnetic and first paleomagnetic study of a primitive achondrite group. We determined that metal inclusions inside silicate grains consist of two magnetic minerals, kamacite and tetraenaite, which have robust recording properties. However, the mechanisms and timing by which these minerals acquired any natural remanent magnetization are unknown. Despite this, Acapulco has not been substantially remagnetized since arriving on Earth and therefore should retain a record dating to 4.55 billion years ago. Future studies could characterize this record by using high-resolution magnetometry measurements of individual populations of grains and developing an understanding of how and when they became magnetized. Our discovery of tetraenaite in ALs provides the first mineralogical evidence for slow cooling [$<5\text{--}10 \times 10^3^{\circ}\text{C}$ per million years (Ma^{-1})] of the AL parent body at low temperatures ($\sim 320^{\circ}\text{C}$). Its presence suggests the AL parent body is unlikely to have been catastrophically disrupted at AL peak temperatures ($\sim 1,200^{\circ}\text{C}$) without subsequent reaccretion.

Plain Language Summary Primitive achondrites are a rare variety of meteorites that formed as the result of limited melting on their parent bodies. They therefore provide key insights into the stages of segregation of metal and rocks in early solar system bodies. However, the sizes and structures of these parent bodies remain uncertain. Here, we conduct a rock magnetic study of the Acapulco acapulcoite to identify the magnetic recorders and to determine if the meteorite could retain a ~ 4.55 billion year old magnetic record. We find that sub-micrometer sized iron-nickel grains embedded in silicate grains should retain a stable magnetization. The presence of high-Ni iron grains suggests acapulcoites cooled slowly at low temperatures, indicating that the parent body could not have been catastrophically disrupted without later reaccretion.

1. Introduction

Meteorites are divided into three classifications. Chondrites are unmelted accretional aggregates of nebular materials, achondrites are melts associated with igneous differentiation on their parent bodies, and primitive achondrites are melt residues from parent bodies that underwent incomplete differentiation (Weisberg et al., 2006). Collectively, they provide records of the thermochemical and geophysical evolution of planetesimals, the <500 km radius rocky-icy parent bodies that served as the building blocks for the planets (Weiss & Elkins-Tanton, 2013). It is typically assumed that many (or perhaps even all) achondrites formed from melting of materials that once formed chondrites. As such, primitive achondrites are of interest because they represent intermediate stages of differentiation and therefore contain unique records of the timescales and mechanisms by which planetary melting processes transformed nebular material into compositionally segregated structures.

Writing – original draft: Elias N. Mansbach, Benjamin P. Weiss
Writing – review & editing: Elias N. Mansbach, Benjamin P. Weiss, Neesha R. Schnepf, Eduardo A. Lima, Cauê S. Borlina, Nilanjan Chatterjee, Jérôme Gattacceca, Minoru Uehara, Huapei Wang

The acapulcoites-lodranites (ALs) are a clan of primitive achondrites composed of two meteorite groups, the acapulcoites and the lodranites. Acapulcoites have bulk near-chondritic compositions that are depleted in Fe-Ni-S melt (<5 vol.% partial melting), average grain diameters of 150–230 μm , and equigranular textures with abundant triple junctions (Keil & McCoy, 2018; McCoy et al., 1996). Acapulcoite mineralogy consists mostly of olivine, pyroxenes, plagioclase, and Fe-Ni-S compounds (Keil & McCoy, 2018; Palme et al., 1981). Some acapulcoites possess mm-to cm-scale metal veins likely representing the initial stages of melt migration on the parent body (Keil & McCoy, 2018; McCoy et al., 1997). They are estimated to have reached peak temperatures of 980–1,170°C during prograde metamorphism (Keil & McCoy, 2018; McCoy et al., 1996), and have metallographic cooling rates 10^3 – 10^5 °C Ma^{-1} (million years) from 350 to 600°C (Keil & McCoy, 2018). Lodranites are coarser grained than acapulcoites (average grain diameter 540–700 μm), also depleted in Fe-Ni-S melt, and are sometimes additionally depleted in plagioclase-pyroxene (5–20 vol.% partial melting), indicating that they were heated to higher temperatures (1,150–1,200°C) (Bild & Wasson, 1976; Keil & McCoy, 2018; McCoy et al., 1996). They have metallographic cooling rates on the lower end of the acapulcoite range, generally 10^3 °C Ma^{-1} at 350–600°C (Keil & McCoy, 2018). The combination in ALs of a near-chondritic composition largely undepleted in incompatible elements and textural evidence for subsolidus recrystallization with limited melting is the hallmark of a primitive achondrite group. ALs are thought to represent a single, distinct parent body from known meteorites based on their unique oxygen isotope compositions and abundances of volatiles, lithophile, and siderophile elements (Greenwood et al., 2012, 2017; Keil & McCoy, 2018).

The metal in the eponymous acapulcoite Acapulco, which comprises 11.3–22.7 wt.% of the meteorite (Palme et al., 1981; Zipfel et al., 1995), has been reported to occur in two forms: (a) composite 50–500 μm -sized assemblages of kamacite ($\alpha\text{-Fe}_{1-x}\text{Ni}_x$ for $x < 0.06$) and zoned taenite ($\gamma\text{-Fe}_{1-x}\text{Ni}_x$ for $0.06 \leq x \leq 0.5$) located interstitially between silicate grains; and (b) sub- μm to μm -sized kamacite and taenite inclusions in the cores of olivine and pyroxene grains (inclusion average $x = 0.08$), henceforth called metal-bearing silicates (MBSs) (Figure 1) (El Goresy et al., 2005; Keil & McCoy, 2018; Palme et al., 1981; Zipfel et al., 1995). The carriers of any remanent magnetization have not been identified in Acapulco but could possibly be kamacite in interstitial metal assemblages (form 1), inclusions in MBSs (form 2) and/or tetrataenite ($\gamma\text{-Fe}_{0.5}\text{Ni}_{0.5}$) in the high-Ni rims of zoned interstitial taenite (form 1) and MBSs (form 2). Tetrataenite forms from the reordering of taenite at 320°C at cooling rates $< \sim 5,000$ °C Ma^{-1} (Yang & Goldstein, 2004), which is within the estimated 10^3 – 10^5 °C Ma^{-1} metallographic cooling rate range of acapulcoites at 350–600°C (Keil & McCoy, 2018). MBSs are of great interest for possible paleomagnetic studies because they resemble dusty olivine chondrules (DOCs) that have been found to be high-fidelity magnetic recorders in LL and CO chondrites due to their fine metal grain sizes (Borlina et al., 2021; Fu et al., 2014).

Despite the extensive petrological, geochemical, and geochronological analyses of ALs, the size, structure, and thermal history of their parent body remain poorly constrained. Previous thermal modeling suggests that ALs formed in the upper 25 km of a body with a radius of 35–270 km that may have had an Fe-Ni-S core (Golabek et al., 2014; Neumann et al., 2018; Touboul et al., 2009). Differences in cooling rates determined by geochronometers and mineral indicators have led to suggestions the parent body was disrupted while ALs were above ~ 500 °C and then potentially reaccreted (Göpel & Manhès, 2010; Lucas et al., 2022), although an alternate explanation might be the unroofing of overlying material as suggested for IVA irons (Yang et al., 2007). Paleomagnetism can be used to search for evidence of a dynamo magnetic field, which would be direct evidence that the body possessed an advecting, liquid metal core with a diameter of at least several tens of km (Bryson et al., 2019; Weiss et al., 2010). A past dynamo would further suggest that at the time of magnetization acquisition, at least the central portion of the parent body efficiently segregated metal and silicates.

The goal of this study is to address the following questions for Acapulco: (a) Does Acapulco retain a pre-terrestrial natural remanent magnetization (NRM) or has the meteorite been substantially magnetized since falling to Earth?; (b) Does Acapulco retain an interpretable early solar system magnetic record to the present day?; and (c) Can the paleomagnetism and rock magnetic properties of Acapulco constrain the parent body's interior structure and thermal evolution? To answer these questions, we inventory the ferromagnetic mineralogy of the meteorite and constrain its recording properties, its form of NRM [e.g., thermoremanent magnetization (TRM), crystallization remanent magnetization (CRM), and/or shock remanent magnetization (SRM)], and at what temperature that NRM could have been acquired. We address the above questions for both the large interstitial metal grains in bulk samples and the metal inclusions in MBSs. While there has been an initial study of the rock magnetic properties of primitive achondrites (Rochette et al., 2009) and a paleomagnetic study of IAB

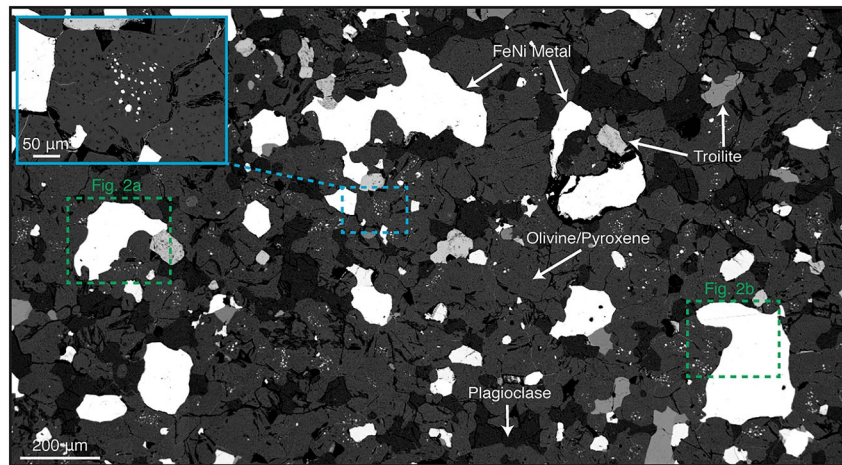


Figure 1. Backscattered electron (BSE) image of Acapulco thin section USNM 5967-1 showing FeNi metal, troilite (FeS), plagioclase, and olivine and pyroxene. The multidomain, interstitial metal grains (50 μm –1 mm in size) dominate the NRM of the bulk samples, making them nonideal magnetic recorders. Blue outlined inset shows a metal-bearing silicate (MBS). Visible in the MBSs are $<10 \mu\text{m}$ FeNi metal grains that may extend into the single domain (SD) or pseudo-single domain (PSD) size range and therefore may have optimal magnetic recording properties. Grains outlined in green dashed boxes are shown in more detail in Figure 2.

iron meteorites (Nichols et al., 2018), which have been proposed to originate from the same parent body as the winonaite primitive achondrite group, no paleomagnetic study has previously been conducted on a primitive achondrite meteorite.

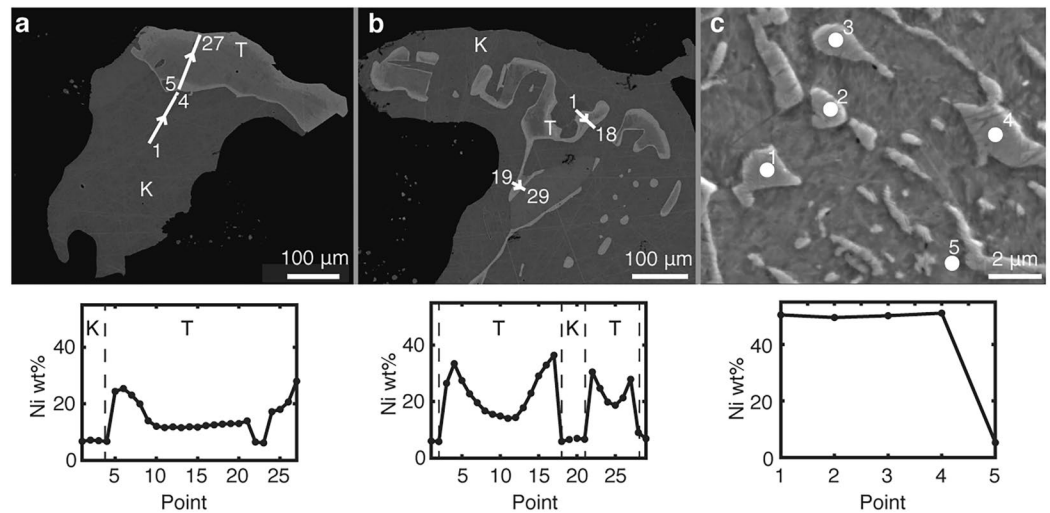


Figure 2. Electron microscopy images and compositions of interstitial metal. (a) BSE image (top) and corresponding WDS measurements (bottom) of an interstitial metal grain (left dashed green box in Figure 1). White line with arrows in the BSE image shows location and direction of the WDS transect. Brightness denotes atomic number, with Fe darker than Ni. These data show that the metal grain is a composite of at least two phases. The bottom section of the grain is uniform in texture and composition with a mean Ni content of 6 wt.%, indicating it is kamacite. The top portion exhibits higher Ni and a zoned composition reaching up to ~ 30 wt.% Ni in the rim and down to ~ 13 wt.% Ni in the center. (b) BSE image of another interstitial metal grain (top) and corresponding WDS transects cover two Ni gradients in a zoned taenite (right dashed green box in Figure 2). The maximum and minimum Ni compositions are 37 and 7 wt.%, respectively. (c) Secondary electron image of plessite in the center of a zoned taenite in an interstitial metal grain (not shown in Figure 1). The precipitates are composed of ~ 50 wt.% Ni, and therefore taenite or tetraetaenite, while the matrix is ~ 5 wt.% Ni and therefore kamacite. *K* = kamacite, *T* = taenite.

2. Materials and Methods

2.1. The Acapulco Meteorite

We selected Acapulco for analysis because previous studies indicated it may have rock magnetic properties favorable for paleomagnetism. In particular, it is one of only two known AL falls and therefore unlikely to have been weathered on Earth [Acapulco has little to no reported weathering products (Dhaliwal et al., 2017)] or exposed to a hand magnet from a collector (Vervelidou et al., 2023; Weiss et al., 2010). Also, Acapulco retains a fusion crust, which can be used to determine whether the interior of the sample has been remagnetized through a fusion crust baked contact test (see below) (Weiss et al., 2010).

Additionally, Acapulco is essentially unshocked [stage S1 (Palme et al., 1981)]. For the average elongation of kamacite grains in Acapulco (see Text S2 in Supporting Information S1), whose magnetic anisotropy should be dominated by shape, the minimum pressure needed for stress anisotropy to overcome shape anisotropy is 6.4 GPa. For tetrataenite, which is dominated by magnetocrystalline anisotropy, the minimum pressure is 97 GPa (See Text S6 in Supporting Information S1). We also note that analog experiments on FeNi-bearing ordinary chondrites indicate that less than half of a saturating isothermal remanent magnetization (IRM) is lost at pressures up to 1.8 GPa (Bezaeva et al., 2022; Gattacceca et al., 2010). Lastly, we do not observe the presence of Neumann bands, which form from shocks $> \sim 1.5$ GPa (Ohtani et al., 2022), in etched FeNi metal grains in Acapulco. Therefore, it is unlikely that Acapulco was remagnetized or demagnetized through shock.

Furthermore, Acapulco is a promising meteorite for paleomagnetic analysis as $^{40}\text{Ar}/^{39}\text{Ar}$ dating of plagioclase yields ancient ages of $4,554 \pm 43$ Ma (Renne, 2000). For cooling rates between 100 and $100,000^\circ\text{C Ma}^{-1}$, the Ar closure temperature for ~ 100 – 200 μm -sized plagioclase is 300 – 400°C , which is well below the Curie temperature of kamacite (780°C) and spans the ordering temperature of tetrataenite (320°C). Thus, the $^{40}\text{Ar}/^{39}\text{Ar}$ age places a lower bound on the date of any NRM acquisition by kamacite and an upper bound for NRM acquisition by tetrataenite. The ancient $^{40}\text{Ar}/^{39}\text{Ar}$ age also suggests that the samples have not experienced significant metamorphism or impact heating since initial cooling (Palme et al., 1981).

For this study, a 4.02 g piece of Acapulco (USNM 5967) with a fusion crust was provided by the Smithsonian National Museum of Natural History. This sample has a fusion crust on one side that extends < 0.5 mm into the interior. From this main mass, we extracted nine mutually oriented bulk subsamples (masses 5–50 mg), labeled NMMAC1-8 and NMMAC12, containing MBSs and interstitial metal grains. These were cut from the main mass in a transect perpendicular to the fusion crust to sample both the crust and the interior of the sample (Figure S1 in Supporting Information S1). Three subsamples (NMMAC 1, 5, and 12) contained fusion crust and the other six (NMMAC 2–4, and 6–8) sampled the interior at various distances up to a maximum of 7.5 mm from the fusion crust. All samples were photographed and mutually orientated to within 5° uncertainty. In addition to the bulk subsamples, seven MBSs labeled MBS 2–5, 8–10 (masses $\sim 0.12 \pm 0.06$ mg) were extracted from a thick section NMMAC11 (Figures S2 and S3 in Supporting Information S1). The MBSs were also photographed and mutually oriented relative to each other and the bulk samples within 5° uncertainty. We acquired the transect of bulk subsamples from the fusion crust into the interior to determine if the meteorite has been remagnetized after falling to Earth. In particular, because the fusion crust is expected to have acquired a TRM from atmospheric heating, if the meteorite has been remagnetized since landing on Earth (e.g., via a hand magnet, weathering and/or viscous remagnetization in Earth's field), the magnetization directions of the fusion crust and the interior subsamples would be clustered.

In addition to a bulk sample, a 30- μm thin section of Acapulco (USNM 5976-1) was provided by the Smithsonian National Museum of Natural History. The thin section was used primarily to determine the size, texture, habit and composition of the metal grains in Acapulco.

2.2. Compositional and Morphological Methods

We collected backscattered electron (BSE) microscopy images and quantitative compositional measurements of polished MBSs and interstitial metal grains using wavelength dispersive spectroscopy (WDS) on a JEOL JXA-8200 Superprobe electron microprobe machine in the Department of Earth, Atmospheric, and Planetary Sciences at MIT. Following WDS measurements but prior to BSE imaging, the samples were etched with 2% nital for 20 s to enhance grain boundaries associated with metallographic exsolution textures. Additional secondary

electron (SE) images and quantitative compositional measurements using electron dispersive spectroscopy (EDS) were acquired using a Merlin Zeiss Field Emission Gun-SEM in the MIT Material Resources Laboratory. All BSE images and EDS and WDS measurements were conducted on thin section USNM 5967-1. In addition, the morphology and sizes of the metal inclusions in MBSs were determined via transmission X-ray microscope imaging at the National Synchrotron Light Source II (Beamline X8C) at Brookhaven National Laboratory (beam energy 7.2 keV, see Text S2 in Supporting Information S1) (Wang et al., 2015).

2.3. Magnetic Methods

We conducted nearly all magnetic measurements in the Massachusetts Institute of Technology (MIT) Paleomagnetism Laboratory. A 2G Enterprises Superconducting Rock Magnetometer (2G SRM) 755 [2σ noise floor of 0.99×10^{-12} Am²; Figure S5 in Wang et al. (2017)] equipped with an automatic sample handling and coil system was used for alternating field (AF) demagnetization of bulk and MBS sample NRM. Bulk samples were AF demagnetized up to a maximum of 85 or 145 mT in steps of 0.5–1 mT and their magnetizations were measured using the 2G SRM. The magnetizations were measured after AF application the along x , y , and z axes (ending with z) once, and then again after AF application along the x , y , and z axes individually twice. The magnetizations within each AF step were then averaged and rotated from the x - y - z 2G SRM coordinate system into a north-east-up sample coordinate frame (Table S3 in Supporting Information S1).

MBS samples were AF demagnetized to up a maximum field ranging between 500–900 mT in intervals of 10–100 mT. Due to the weak NRMs of the MBSs ($\sim 10^{-11}$ – 10^{-12} Am²), we extracted them from the meteorite (see Text S1 in Supporting Information S1) and their magnetizations were measured using a superconducting quantum interference device (SQUID) microscope (noise floor of 6×10^{-15} Am²), which maps the out-of-the-page (z) component of the magnetic field produced by the sample ~ 200 μ m above the MBS (Weiss et al., 2007). The net magnetic moments of MBS samples were determined by performing a dipole fit [dipolarity for the maps were >0.85 (a perfect dipole has a dipolarity of 1) and therefore a multipolar fit was not necessary] to the SQUID microscope maps (Lima & Weiss, 2016). For AF demagnetization up to 145 mT, AF demagnetization was conducted in the x , y , and z directions; following the z -application, SQUID microscope maps were made. Such sequences were repeated and the resulting measured moments averaged to reduce spurious anhysteretic remanent magnetization (ARM) (Tikoo et al., 2012). Between 145 and 420 mT, SQUID microscope maps were made after AF demagnetization along each of the three AF axes; these were used to correct for any gyroremanent magnetization acquired during AF demagnetization by averaging the moments measured after each x - and y -, and z -AF application following the Zijderveld-Dunlop method (Stephenson, 1993). Demagnetization above 420 mT was achieved using IRMs applied via a ASC Scientific Model IM-10 impulse magnetometer in alternating directions and decreasing in strength by intervals of 100 mT (i.e., DC demagnetization). Magnetic optical imaging (MOI) was performed at CEREGE in France. Directions of NRM components and their maximum angle of deviation (MAD) values, which provide a measure of angular uncertainty in the components (Khokhlov & Hulot, 2015), were determined by principal component analysis (PCA) (Kirschvink, 1980).

After NRM AF demagnetization, ARMs were applied to bulk samples (130 mT AC field, 200 μ T bias field) and MBSs (145 mT AC field, 200 μ T bias field) to simulate acquisition of a TRM acquired during cooling (Dunlop & Argyle, 1997). AF demagnetizations of these ARMs were compared to those of the NRMs to determine if the NRMs are consistent with a TRM.

The magnetic recording properties of bulk samples and MBSs were assessed through applications and subsequent AF demagnetizations of IRMs on previously demagnetized samples. We used AF demagnetization of a 1 T IRM both to estimate coercivity spectra, which we used to help identify ferromagnetic minerals, and to constrain the origin of NRM overprints through paleointensity estimations. The apparent paleointensity (B_{int}) was calculated as:

$$B_{\text{int}} = \frac{\Delta \text{NRM}}{\Delta \text{IRM}} \cdot a$$

where ΔNRM and ΔIRM are the change in NRM and IRM respectively during AF demagnetization and $a = 3,000$ μ T is an experimentally determined correction factor to account for the ratio of IRM to TRM for kamacite (Gattacceca & Rochette, 2004). We use the term “apparent” here since this estimate assumes a TRM or viscous remanent magnetization (VRM) carried by kamacite; this likely only applies to the low coercivity (<15 mT) fraction of the NRM of the samples.

Thermal demagnetization of IRM was conducted to aid in ferromagnetic mineral identification in MBSs through determination of Curie points. A 1 T IRM was applied to MBSs 5, 8, and 10 and heating was performed using a Magnetic Measurements oven in a controlled atmosphere to limit alteration or creation of new magnetic minerals during heating (Suavet et al., 2014). Consistent with estimates of the oxygen fugacity for Acapulco formation based on olivine-chromite thermometry (Benedix & Lauretta, 2006), we set the oxygen fugacity to -2.3 log units below that of the iron-wüstite (IW) buffer. Heating was conducted in steps of 10 – 50°C up to 770°C with the full heating and cooling time taking 20 min total for each step.

The location and distribution of the magnetic remanence carriers in MBSs were determined using a quantum diamond microscope, which maps the magnetic field with a ~ 5 μm spatial resolution at a distance of ~ 10 μm above the sample [moment sensitivity 1×10^{-14} Am^2 (Fu et al., 2020; Glenn et al., 2017)].

To search for the presence of tetrataenite in Acapulco, we conducted first order reversal curve (FORC) measurements on an interior unheated bulk sample and on an interior bulk sample previously heated to 600°C for 20 min. Heating above the ordering temperature of tetrataenite results in disordering of the mineral at a rate that increases with temperature (Dos Santos et al., 2015). In particular, at 600°C , tetrataenite is expected to disorder after <5 min (Dos Santos et al., 2015). The loss of tetrataenite should therefore result in the loss of a high-coercivity phase in the FORC diagram as observed in ordinary chondrites (Gattacceca et al., 2014). The FORCs were measured using a vibrating sample magnetometer in the MIT Department of Material Sciences and Engineering. A total of 83 minor loops were measured, varying the field from -0.66 to 1 T in 20 mT steps. The FORC distribution was determined by taking the mixed second derivative of the magnetization curves in H_A – H_B space [H_A is the starting field of each minor loop and H_B is each field step; see Muxworthy and Roberts (2007)]. The FORC diagrams were created using the FORCinel program (Harrison & Feinberg, 2008) with correction and smoothing parameters provided in Text S3 in Supporting Information S1.

3. Results

To address the three questions in Section 1, we conducted electron, optical, transmission X-ray and magnetic microscopy and compositional analyses of the metal in Acapulco, analyzed the magnetic properties of the metal, and studied the NRM of bulk samples and individual MBSs. These three investigations allow us to determine the ferromagnetic mineralogy, the recording properties of the minerals, and whether Acapulco has been magnetized since falling to Earth.

3.1. Microscopy and Compositional Analysis of Acapulco Metal

We found that interstitial metal grains range in size from 50 μm to 1 mm (Figure 1). Our BSE images and WDS transects of thin section USNM 5967-1 show that the interstitial metal grains consist of two phases: (a) kamacite (5 – 6 wt.% Ni) and (b) zoned taenite exhibiting Ni gradients from 13 wt.% near the center of the grains to 37 wt.% near the rim (Figures 2a and 2b). The zoning is consistent with the “M” shaped profile seen in iron meteorites that forms during subsolidus cooling due to the slower diffusion of Ni through taenite compared to kamacite (Yang & Goldstein, 2005). We did not observe any cloudy zone microstructures in BSE images of the thin section down to ~ 20 nm resolution after nital etching or in magneto-optical images (Figures S5, S6 in Supporting Information S1).

BSE images of the center of zoned taenite interstitial metal grains show the presence of plessite, a metallic micro- and/or nanostructure that forms from the subsolidus decomposition of martensite (α_2 -FeNi) into high- and low-Ni phases [Figure 2c, (Goldstein & Michael, 2006)]. EDS spot measurements of the μm -sized high-Ni precipitates show that their Ni contents reach up to ~ 50 wt.% and therefore should be in the form of either taenite or tetrataenite.

Transmission X-ray microscopy shows that unlike the >50 μm interstitial metal grains, MBSs possess inclusions with sizes <0.4 – 13 μm (Figure S4 in Supporting Information S1). BSE images show that MBS metal grains consist of two types: (type I) a low-Ni FeNi metal phase with some grains possessing a <1 μm , high-Ni rim (Figures 3a and 3b), and (type II) an intergrowth of high-Ni precipitates in a low-Ni matrix (Figures 3b and 3c). Our WDS measurements of type I grains (Figure 3b) show that the low-Ni phase is kamacite (<6 wt.% Ni) and that the high-Ni rim, which can reach up to ~ 50 wt.%, is either taenite or tetrataenite. No Ni compositional gradient is observed in these grains.

Type II metal grains exhibit a plessitic microstructure similar to that observed in the interstitial metal grains, although on a smaller scale (generally sub- μm precipitates compared to the μm -sized precipitates in the interstitial

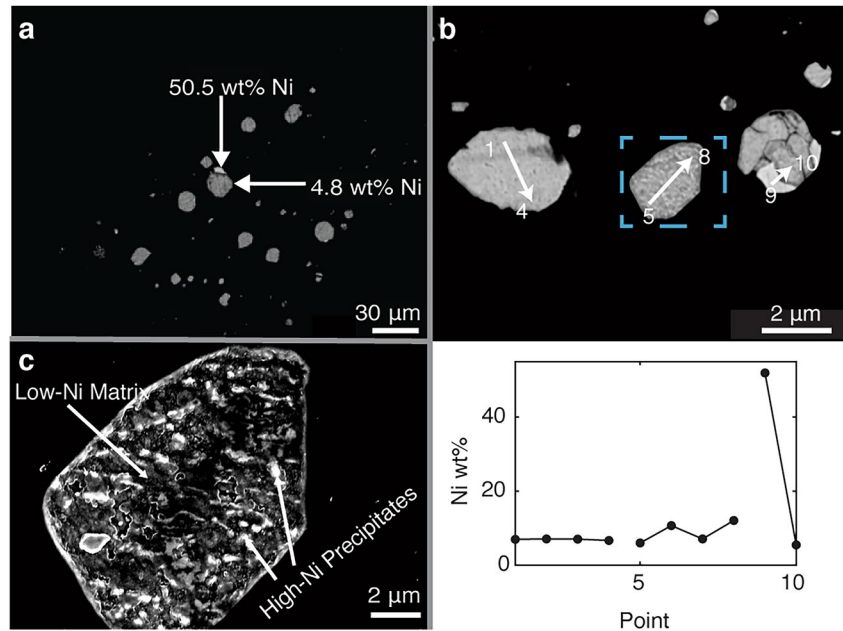


Figure 3. Microscopy images and compositions of MBS metal. (a) BSE image of metal inclusions in an MBS. Most inclusions have apparently homogenous Ni abundances in the range of kamacite with occasional inclusions (<1% of total area) possessing brighter, high-Ni rims [type I grains]. These grains have not been etched with nital. (b) Top: BSE image of metal inclusions in a separate MBS from (a) showing two type I grains on the far left and right and a type II grain in the center. The grains have been etched with nital. Dashed blue box shows location of zoomed BSE image in (c). Bottom: WDS compositions at the locations marked in the BSE image. (c) Zoomed BSE image of the boxed metal inclusion in (b) showing a plessitic microstructure.

metal). Although the small sizes of the precipitates prohibit determination of their composition by EDS and WDS, it is likely that as for plessite in the interstitial grains, some metal grains in the MBS plessite have compositions reaching ~50 wt.% Ni given that such a Ni-rich composition is a natural outcome of plessite formation during slow cooling (Goldstein & Michael, 2006).

3.2. NRM Demagnetization

We analyzed the NRMs of nine mutually oriented bulk subsamples (5–50 mg) of fusion-crust specimen USNM 5967 (labeled NMMAC1–8, 12; Figure S1 in Supporting Information S1) in a transect from the exterior to the interior. Our AF demagnetization revealed that three fusion-crust samples each possessed a common low coercivity (LC) component, denoted LCf, that unblocked between 0 and 3–14 mT depending on the sample (Figures 4a and 4c; Figure S11 in Supporting Information S1). Similarly, all interior bulk samples had a common LC component, denoted LCi, that unblocked between 0 and 5–15 mT (Figures 4b and 4d; Figure S11 in Supporting Information S1). While all bulk samples had a LCi or LCf component, the high average MAD values of 16.8° for these components indicate large directional scatter during demagnetization over the component AF ranges. None of the LCf or LCi components for the fusion-crust or interior samples have a deviation angle (DANG) less than their MAD value (Tauxe & Staudigel, 2004), suggesting they are not origin-trending and therefore not primary components (Table S3 in Supporting Information S1).

The average directions of the LCi and LCf components are 58.8° apart and do not fall within each other's 95% confidence circles (Figure 4e). Because the LCi and LCf α_{95} ellipses overlap, we conducted a common mean bootstrap test (Tauxe, 2010) to determine if the groups of LCi and LCf components share average directions. The two distributions failed the test, indicating that their mean directions are statistically distinct to 95% confidence. Out of the nine samples, we estimated paleointensities for six samples. The paleointensities of the LCf components for the fusion-crust samples NMMAC1 and NMMAC12 are $82.1 \pm 15.7 \mu\text{T}$ (uncertainties here and elsewhere are 95% confidence intervals) and $79.9 \pm 20.3 \mu\text{T}$, respectively, assuming that the LC components are carrying a VRM or TRM. The average paleointensity of the four LCi components calculated for interior samples NMMAC2, NMMAC3, NMMAC7, and NMMAC8 is $42.2 \pm 23.1 \mu\text{T}$ (Table S3 in Supporting Information S1).

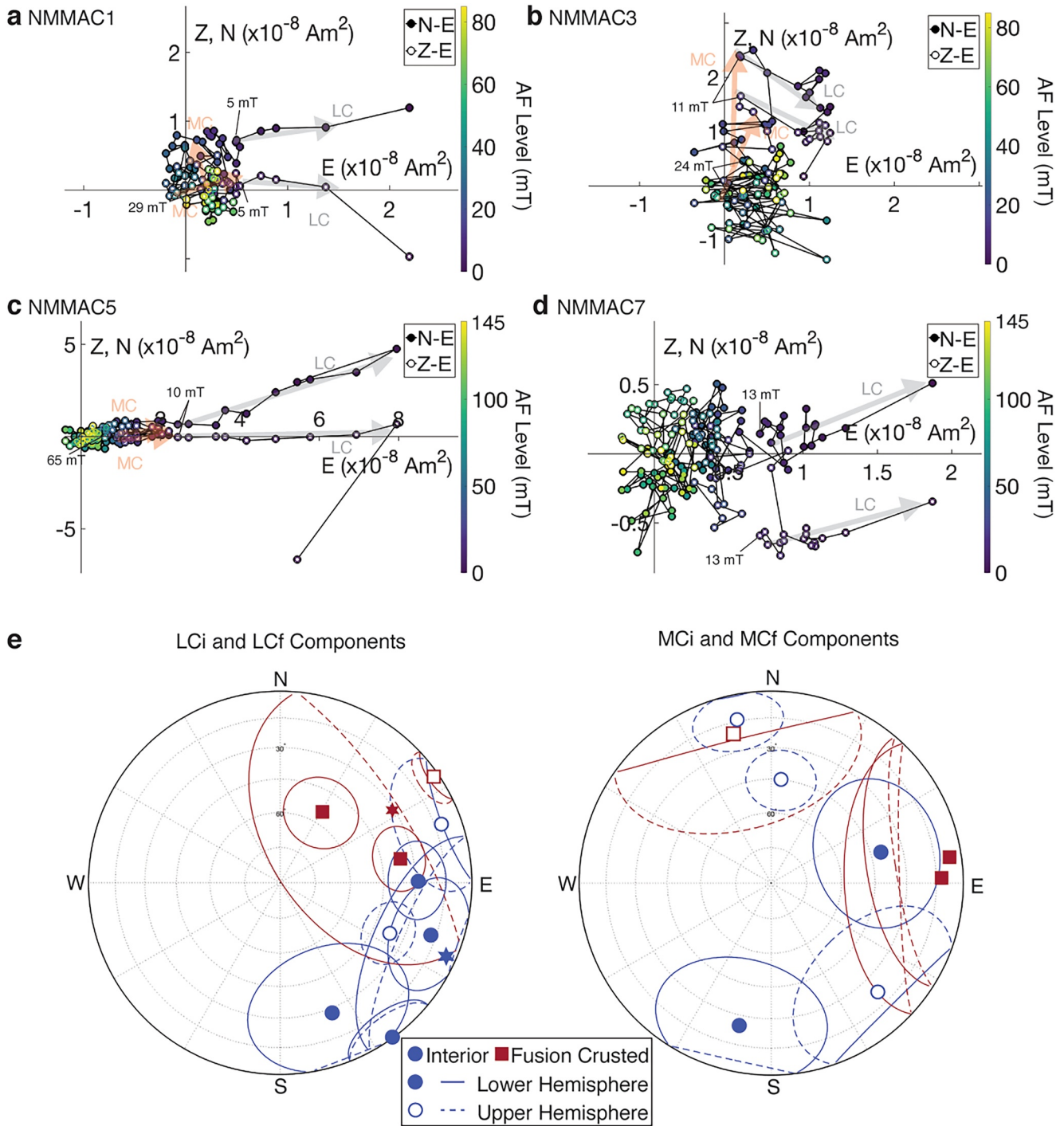


Figure 4. AF demagnetization of bulk sample NRM vectors measured with the 2G SRM. (a)–(d) Orthographic projections of endpoints of NRM vectors onto the north-east (N–E) and up-east (Z–E) planes. LCI/LCf components are denoted by the gray arrows and MCi/MCf components are denoted by the orange arrows. (a) Fusion-crusted sample NMMAC1: an LCf component unblocked between 0 and 4.5 mT and an MC component unblocked between 5.5 and 29 mT. (b) Interior sample NMMAC3: an LCI component unblocked between 0 and 10 mT and an MC component unblocked between 11 and 24.5 mT. (c) Fusion-crusted sample NMMAC5: An LCf component unblocked between 0 and 14 mT and an MC component unblocked between 14.5 and 66 mT. (d) Interior sample NMMAC7: an LCI component unblocked between 0 and 13 mT. Color bars in (a)–(d) denote AF level for each step. (e) Equal area stereographic projection showing LCI/LCf (left) and MCi/MCf (right) component directions for the bulk samples. Fusion-crusted samples are denoted as red squares and interior samples as blue circles. The average fusion-crusted LC direction (red star) and average interior sample LC direction (blue star) fall outside each other's 95% confidence circles, but their confidence circles overlap.

We found that seven of the nine bulk samples possessed a medium coercivity component (denoted MCi for interior samples and MCf for fusion-crust samples) that unblocked starting from the end to the LCi/LCf component to 10–66 mT depending on the sample. After removal of the MCf and MCi components, there were no further identifiable trending components in any sample. We note that no effects were seen from gyroremanent magnetization at large demagnetization fields for any sample [e.g., (Garrick-Bethell et al., 2009)].

Unlike the LCi and LCf components, the individual MCi and MCf component directions are not well-clustered (Figure 4e). Two of the fusion-crust samples (NMMAC5 and 12) show similar (9° difference) MCf component directions, but the direction of the third fusion-crust MCf differs by 106°. The average MAD of the MCi and MCf components is 31.9°, highlighting the scatter in the demagnetization of the samples despite noticeable magnetization trends. The MCf components of bulk samples NMMAC1, 5, and 12, and the MCi component of bulk sample NMMAC6 have $DANG < MAD$, suggesting they may be origin-trending (Table S3 in Supporting Information S1). However, the MAD values of these components are $>30^\circ$, and therefore the components are unlikely to be a primary magnetic record.

AF demagnetization of the NRM of five MBSs did not reveal any clear components, although MBS3 and MBS9 may possess a weak LC component (Figures 5a–5c; S12). The moments of each sample did not exhibit consistent decreases in intensity. Instead, they were clustered (Figure 5b) and/or inconsistently jumped in direction with each AF step (Figure 5c). Similar to the bulk samples, no effects were seen from gyroremanent magnetization. The NRM directions of the MBSs prior to AF demagnetization (Figure 5d) are scattered and not consistent with the LCi or LCf directions.

3.3. Magnetic Properties

AF demagnetization of a saturating 1 T IRM applied to two fusion-crust samples, NMMAC1 and NMMAC12, and two interior samples, NMMAC6 and NMMAC7, revealed different behaviors (Figure 6a). The fusion-crust samples show a rapid decrease in magnetization at lower AF levels, dropping to 50% of their IRM moment (known as the median destructive field [MDF]) at 9 and 14.5 mT for NMMAC12 and NMMAC1 respectively. Comparatively, the interior samples show a slower rate of decrease in moment with AF level and MDFs of 30 and 47 mT for NMMAC7 and NMMAC6, respectively.

By the 130 mT AF step, the two interior samples still retained 19%–25% of their original IRM while the fusion-crust samples had less than 1% of their IRM, indicating that the interior samples contain a larger fraction of recorders with microcoercivities >130 mT (Figure 6a). This behavior is also seen in the coercivity spectra of the samples (Figure 6b), calculated as the derivative of the curve in Figure 6a with respect to AF level: the fusion-crust samples have a factor of 2 larger rate of magnetization loss per AF level compared to the interior samples. However, both interior and fusion-crust samples only show a peak in their coercivity spectra at low AF levels, suggesting that their magnetizations are carried primarily by lower-coercivity grains.

The AF demagnetization behavior of ARMs also differed for fusion-crust samples (Figure 6c) compared to interior samples (Figure 6d). Fusion-crust samples showed a monotonic decrease in moment until ~ 50 mT, after which the moment fluctuated around a constant value. By comparison, the ARMs for the interior samples (Figure 6d) experienced monotonic decreases in moment until AF levels of 10–30 mT depending on the sample, after which their moments showed no further demagnetization with increasing AF level.

The FORC diagram on unheated interior sample NMMAC6 (Figure 8) revealed the presence of a vertically spread, high coercivity signal extending beyond 700 mT consistent with tetrataenite in the cloudy zone (Blukis et al., 2020). This is somewhat surprising because this microstructure is not observed in our BSE images, perhaps due to their ~ 20 nm SEM resolution. In addition, there is a strong signal consistent with multidomain kamacite and an asymmetry below the horizontal axis that may be due to interactions between the higher-coercivity tetrataenite and the lower-coercivity kamacite in plessite (Gattacceca et al., 2014). After heating interior sample NMMAC7 to 600°C, the high-coercivity signal is replaced by a central ridge extending out to ~ 500 mT (Figure 8), which is consistent with kamacite in DOCs (Lappe et al., 2011) rather than tetrataenite. The loss of the high-coercivity signal after heating to 600°C is consistent with the disordering of tetrataenite as has been observed previously in tetrataenite-bearing ordinary chondrites (Dos Santos et al., 2015; Gattacceca et al., 2014).

Quantum diamond microscopy (Glenn et al., 2017) confirms that the main magnetization carriers of the MBSs are metal inclusions in the grain interiors (Figure S9 in Supporting Information S1). AF demagnetization of a

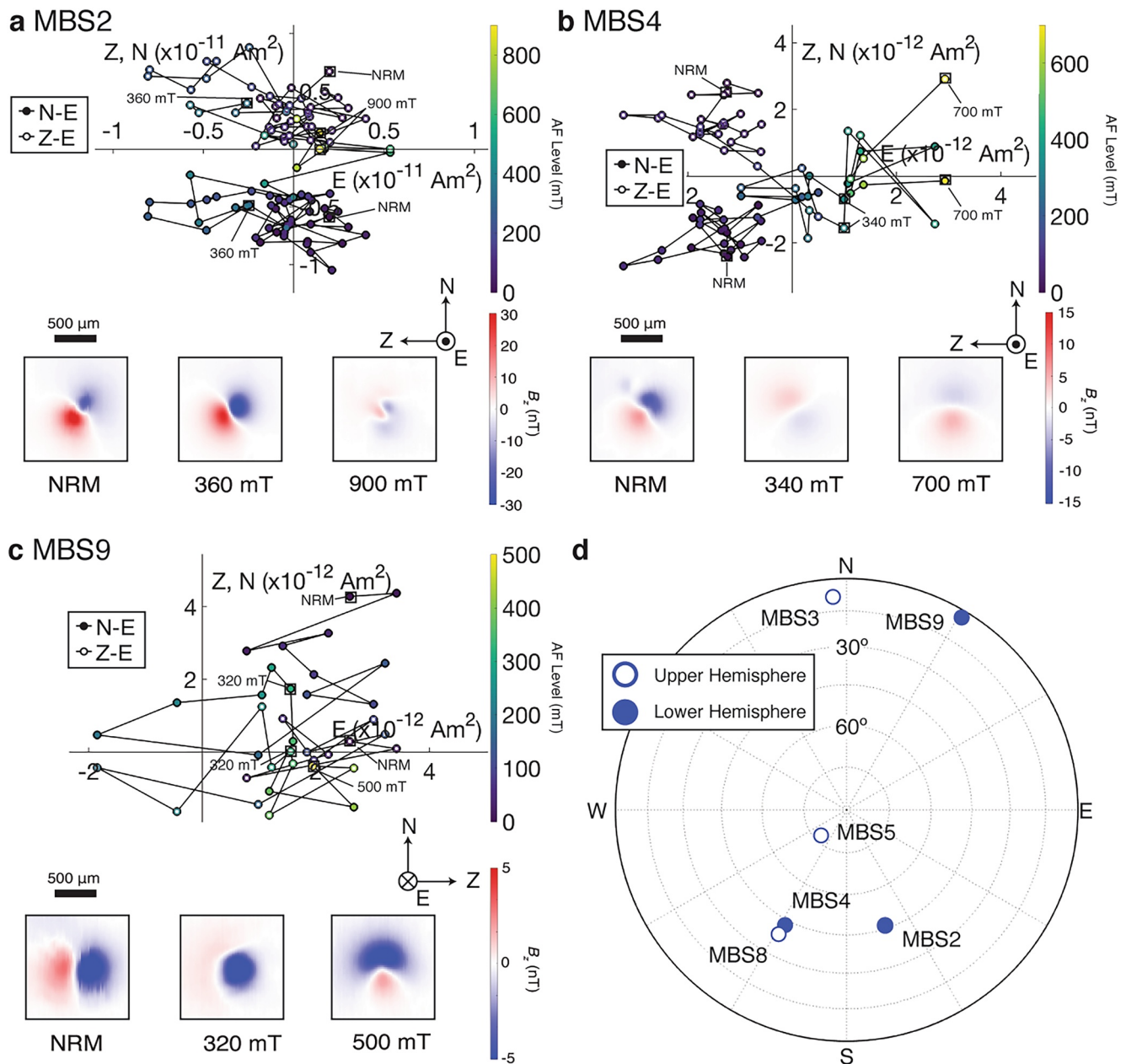


Figure 5. NRM demagnetization of MBSs as measured in the SQUID microscope. (a)–(c) Orthographic projections of endpoints of NRM vectors onto the northeast (N–E) and up-east (Z–E) planes: MBS2 (a) MBS4 (b) and MBS9 (c). Representative SQUID microscope maps at selected field steps for each MBS are shown below and are associated with boxed steps on the orthographic projections. These maps show the vertical component of the magnetic field ~ 0.2 mm above the sample, compasses show orientation of maps. (d) Equal area stereonet showing the NRM direction of MBSs. Open (closed) circles represent NRM directions in the upper (lower) hemisphere of the stereonet.

1 T IRM for MBSs 4, 5, and 8 shows that the silicates retain >22–41% of their initial IRM after being demagnetized to 120 mT (Figure 7a). The average MDF of the three MBSs is 65.1 mT, 5.5 and 1.7 times higher than the average MDFs for the fusion-crust bulk samples and interior bulk samples, respectively. Previous AF demagnetizations of 1 T IRMs in DOCs indicate they retain only 8%–24% of their IRM after being demagnetized to 120 mT (Figure 7a). Thus, there is a population of grains in MBSs with microcoercivities exceeding the maximum coercivities observed for DOCs, which are amongst the highest fidelity known magnetic recorders for chondrites (Borlina et al., 2021; Fu et al., 2014; Lappe et al., 2011, 2013). However, the higher rate of loss of magnetization between 0 and 90 mT for MBSs compared to DOCs suggests that MBSs have a larger fraction

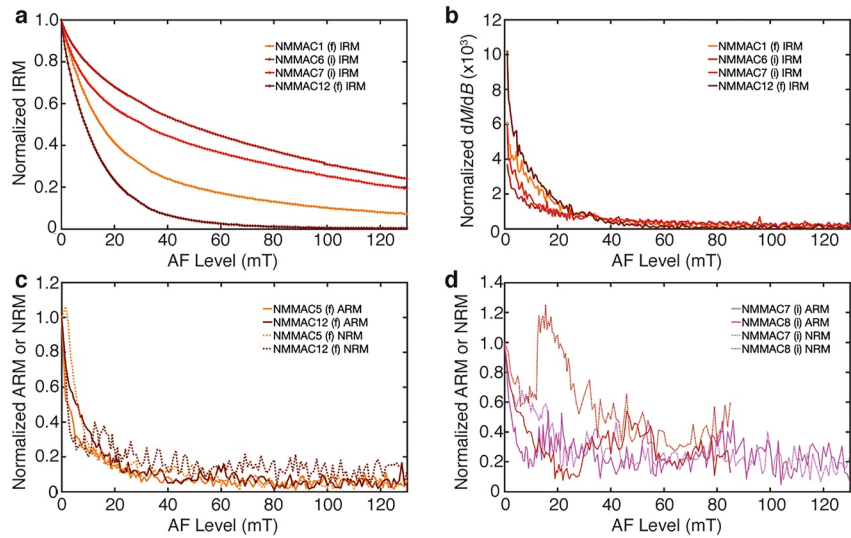


Figure 6. AF demagnetization of IRM and ARM in bulk samples using the 2G SRM. For all figures, (i) and (f) in the legend denote interior and fusion-crusted samples respectively. (a) Normalized IRM demagnetization as a function of AF level. (b) IRM coercivity spectrum calculated by taking the derivative of the data in (a) with respect to AF level. (c) Normalized ARM demagnetization (solid line) and normalized NRM demagnetization (dashed line) vs. AF level for two fusion-crusted samples. (d) Normalized ARM demagnetization (solid line) and normalized NRM demagnetization (dashed line) vs. AF level for two interior samples.

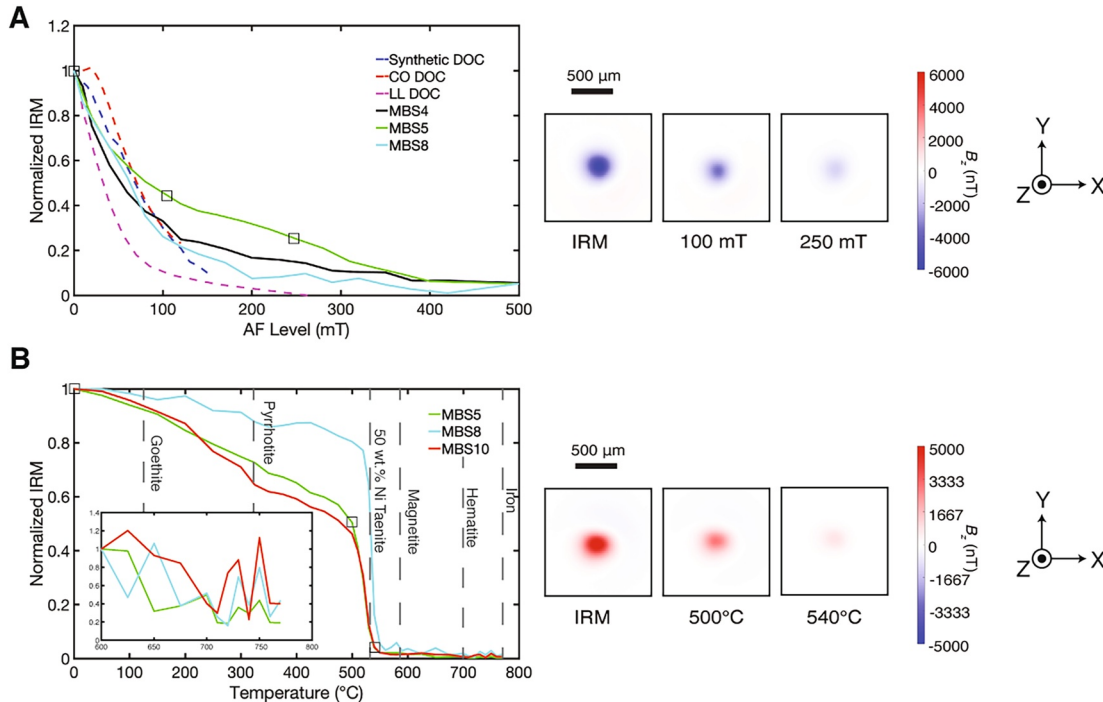


Figure 7. Demagnetization of IRM in MBSs using SQUID microscopy. (a) AF demagnetization of a 1 T IRM for MBSs 4, 5, and 8 compared to a synthetic DOC (Lappe et al., 2011), type 3.00 CO (Dominion Range 08,006) DOC (Borlina et al., 2021), and type 3.00 LL (Semarkona) DOC (Fu et al., 2014). Representative SQUID microscope maps showing the out-of-the-page component of the magnetic field at a height of 200 μm above the sample at selected field steps for MBS 5 are shown. The IRM was applied in the into-the-page ($-z$) direction. (b) Thermal demagnetization of a 1 T IRM for MBSs 5, 8, and 12. The Curie temperatures of various ferromagnetic phases are shown by the dashed gray lines. Representative SQUID microscope maps at selected field steps for MBS 5 are shown. The IRM was applied in the out-of-the-page ($+z$) direction. Inset shows a zoom into the thermal demagnetization from 600 to 770°C. The IRM for each MBS is renormalized to the magnetization at 600°C.

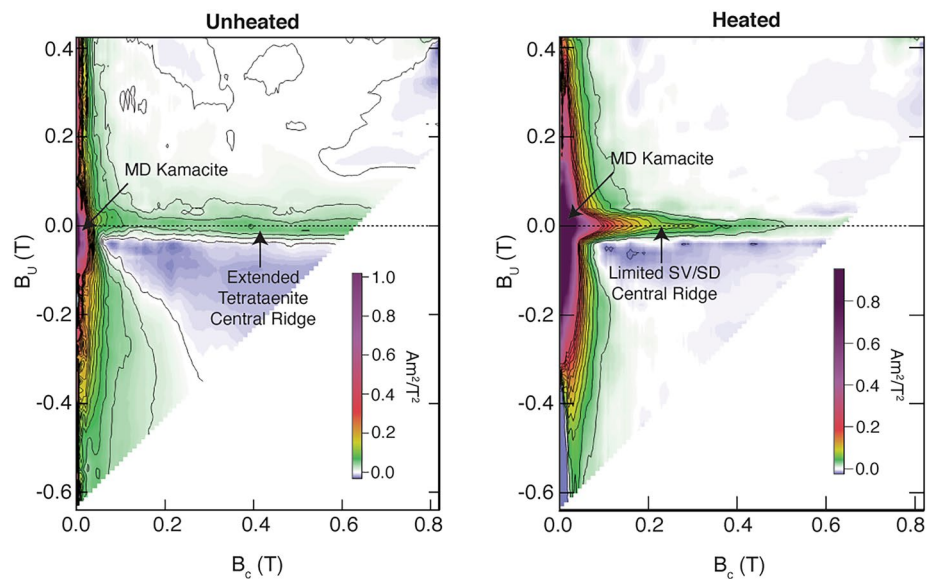


Figure 8. FORC diagrams for unheated bulk interior sample NMMAC6 (left) and bulk interior sample NMMAC7 after heating to 600°C (right). In the unheated sample, a high-coercivity signature is observed that extends beyond 700 mT without evidence for tailing off (tetraenaite), in addition to a strong multidomain kamacite signal. The asymmetry in the low coercivity region is consistent with interactions between tetraenaite and low-coercivity phases. After heating, the high-coercivity tetraenaite signal is lost and transforms into a central ridge that is consistent with kamacite observed in DOCs (Lappe et al., 2011). For ease of viewing, the diagrams are plotted as $B_C = (H_B - H_A)/2$ versus $B_U = (H_B + H_A)/2$.

of metal grains with coercivities below 90 mT, which are very likely the $>1 \mu\text{m}$ metal inclusions visible in BSE images (Figure 1).

Controlled atmosphere thermal demagnetizations of a 1 T IRM applied to three MBSs showed a progressive loss of magnetization in all MBSs during heating from room temperature to 500°C (Figure 7b). The IRM then exhibited a sharp 37%–64% drop between 500 and 540°C, consistent with the Curie temperature of taenite with 49–52 wt.% Ni (Swartzendruber et al., 1991) and/or the loss of IRM from disordering of tetraenaite by laboratory heating (Dos Santos et al., 2015). We favor the latter explanation given the results from the FORC diagrams above that indicate the presence of tetraenaite in an unheated bulk sample and subsequent disordering of tetraenaite after heating to 600°C. Between 600 and 770°C, there is a noisy but noticeable loss in IRM that is likely indicative of kamacite (inset Figure 7b).

4. Discussion and Implications

4.1. Does Acapulco Have a Pre-Terrestrial Magnetic Record?

AF demagnetization of NRMs in bulk samples and MBSs and their comparison to laboratory ARMs and IRMs indicate that Acapulco retains a pre-terrestrial magnetic record. We present three lines of evidence supporting this claim: (a) $\text{NRM}/\text{IRM} < 1.5\%$, (b) directional scatter in MC components in bulk samples (i.e., passed Watson randomness test), and (c) lack of terrestrial weathering products.

The low NRM/IRM values ($< 1.5\%$; Tables S1, S2 in Supporting Information S1) of the MBSs and bulk samples suggest that the interior of Acapulco was not substantially remagnetized by an external field since falling to Earth. Since the expected proportion of magnetic recorders aligned with an Earth-strength external field during cooling (TRM efficiency) is $\sim 1\%$ of saturation IRM (McClelland, 1996; Yu et al., 2007), the NRM/IRM of the samples are consistent with a natural form of magnetization and not artificial contamination (e.g., from a hand magnet), which would produce $\text{NRM}/\text{IRM} > 10\%$ (Vervelidou et al., 2023).

The MCi/MCf components of bulk samples are scattered (Figure 4) and the NRM directions of the MBSs vary in direction as well (Figure 5). This is consistent with a lack of a strong overprint which would align the magnetizations of the bulk samples and MBSs. While curved fields around hand magnets can create NRMs with smoothly

varying directions as a function of depth in a sample and multiple exposures to hand magnets of different strengths from different orientations could create a scatter in the magnetization directions (Vervelidou et al., 2023), the low NRM/IRM values preclude this possibility for Acapulco. This is consistent with Acapulco being a fall given that magnet remagnetization mainly affects meteorite finds [e.g., (Weiss et al., 2008)].

Lastly, thermal demagnetizations of IRMs in MBSs show that the remanence carriers are predominantly FeNi metal alloys (Figure 7b). Common terrestrial phases that could form from weathering and oxidation of meteoritic metal include magnetite, hematite, and goethite (Uehara et al., 2012; Weiss et al., 2010). There is no observed drop in magnetization after heating to the Curie temperatures for those minerals.

While the LCf and LCI directions are statistically distinct and therefore Acapulco technically passes the fusion crust baked contact test, the directions' relative proximity could be interpreted as indicating uncertainty as to whether Acapulco actually passes that test. The proximity in the average directions could be due to a VRM acquired by the low-coercivity metal grains while immersed in Earth's magnetic field prior to NRM demagnetization. This interpretation is supported by the LCI/LCf paleointensities that are consistent with an Earth-strength field. Thus, the interior sample LCI directions would retain the VRM while the fusion-crust LCF directions are an admixture of the VRM and a magnetization acquired during atmospheric entry. We note that the shapes of the fusion-crust samples' ARM and NRM demagnetization curves are similar (Figure 6c), suggesting that the LCF components in the samples are at least partially a TRM. This is expected since the fusion crust was a melt produced during atmospheric entry that cooled in Earth's magnetic field. In contrast, the ARM and NRM demagnetization curves for the interior samples are different: the ARM demagnetizes monotonically up to 10–20 mT while the NRM moment is noisy and does not decline much in magnitude (Figure 6d). Regardless of the fusion crust baked contact test results, the scatter in the MCI/MCF components indicates that the external field source of the LCI/LCf component did not fully magnetize Acapulco.

4.2. Can Acapulco Reliably Retain an Early Solar System Magnetization?

The two major ferromagnetic recorders in Acapulco are kamacite and tetrataenite. Kamacite is clearly identified by its low-Ni composition. We interpret the high-Ni phases in MBSs and the plessitic microstructures to be tetrataenite rather than taenite on account of their high coercivities (>700 mT), changes in sample coercivity after heating, and Ni composition, in addition to further magnetic measurements discussed in the supplement. For bulk interior samples, Acapulco's NRM, ARM, and IRM are dominated by kamacite in the large interstitial metal grains. While there is evidence from our microscopy and magnetic data that tetrataenite is present in the plessitic cores of zoned taenite grains and MBSs, these precipitates' magnetizations are masked by the larger and more abundant kamacite. Kamacite that forms above its Curie temperature will record a TRM upon cooling. However, the morphology of the kamacite and the observed Ni gradients in the interstitial metal grains provide evidence of formation by subsolidus recrystallization of taenite as Ni is diffused out of the crystal structure. Hence, the kamacite in Acapulco would likely have recorded thermochemical remanent magnetization (TCRM), a form of remanence for which reliable paleointensity estimates have not yet been developed (Garrick-Bethell & Weiss, 2010). Furthermore, the various kamacite grains in the interstitial metal likely passed through their blocking temperatures at different times. If a magnetic field was present in the region where ALs formed, the NRM of the bulk samples would be the sum of magnetizations acquired at different periods in time under potentially different field strengths and orientations. This could lead to scattered MCI/MCF directions. We note that the <1.5 GPa shock state of Acapulco indicates that its NRM is almost certainly not an SRM (see Section 2.1) and that it is unlikely to have been substantially demagnetized or remagnetized by shock pressures or heating since 4.55 Ga (Bezaeva et al., 2022; Weiss et al., 2010).

For MBSs, Acapulco's NRM, IRM, and ARM are carried by kamacite and tetrataenite. Tetrataenite would record a CRM during its formation by the reordering of taenite when the meteorite cooled through 320°C (Einsle et al., 2018). Type I grains in MBSs are either present as pure kamacite or show evidence of subsolidus recrystallization in the form of a high-Ni rim. Thus, these grains either recorded a TRM during cooling or a similar TCRM as the kamacite in the interstitial metal grains in the bulk samples. Type II metal grains, which formed from decomposition of martensite into plessite at temperatures <500°C (Goldstein & Michael, 2006), have kamacite and tetrataenite that would record a TCRM. The TCRM for the kamacite would be recorded at the decomposition temperature and the TCRM for tetrataenite would be recorded at and below 320°C. We note that given the metallographic cooling rates reported for Acapulco [10^3 – 10^5 °C Ma⁻¹ at 350–600°C (Keil

& McCoy, 2018)], the time difference between 780°C and 320°C could be 0.005–0.5 Ma. Therefore, similar to the bulk samples, the NRM of the MBSs are likely aggregates of magnetizations produced at different times and possibly different external field conditions. As with the bulk samples, this could lead to scattered NRM and component directions.

Kamacite and tetraenaite that occupy the single domain (SD) or single vortex (SV) states can retain magnetizations stable against viscous relaxation over solar-system timescales (Mansbach et al., 2022; Shah et al., 2018). Electron holography of kamacite inclusions with a range of elongations in a synthetic DOC shows that grains up to ~250 nm occupy the SD or SV state (Lappe et al., 2013). In Acapulco bulk samples, the >50 μm size of the kamacite in the interstitial metal suggests that they are most likely multidomain and therefore poor magnetic recorders. However, sub-μm kamacite grains in MBSs could occupy the SV or SD state.

Based on micromagnetic modeling results, non-interacting tetraenaite occupies the SD state between 6 and ~160 nm depending on its elongation (Mansbach et al., 2022), though we note that interacting tetraenaite grains in the cloudy zone microstructure have been observed to act as SD grains at sizes <~150 nm even when falling outside the predicted SD stability region (Nichols et al., 2020). Unlike kamacite, tetraenaite does not have an SV state and transitions directly from the SD state to a two-domain state due to its high magnetocrystalline anisotropy (Mansbach et al., 2022). The sizes of the tetraenaite grains in the bulk samples (μm) and MBSs (μm to sub-μm) indicate that they are likely multidomain. However, micromagnetic modeling of two-domain tetraenaite shows that the mineral can retain a stable magnetization against viscous relaxation and external remagnetization over the lifetime of the solar system (Mansbach et al., 2022). Therefore, the tetraenaite grains in Acapulco may hold a NRM dating back to near the time of its formation at 4.55 Ga.

4.3. How Can the Paleomagnetism and Rock Magnetic Properties of Acapulco Constrain the Parent Body's Interior Structure and Thermal Evolution?

The identification of tetraenaite provides a powerful cooling rate constraint on the AL parent body. An additional constraint could be derived from the fact that we do not observe cloudy zones in our BSE images. A limitation with the latter is that, as mentioned above, the islands may be smaller than the resolution of the BSE images (<20 nm) [e.g., like those observed in some IVA irons (Yang et al., 2007)] and therefore additional transmission electron microscope analysis is required to confirm the lack of a cloudy zone. We interpret the presence of tetraenaite and the provisional absence of a cloudy zone as follows. Ordering from taenite to tetraenaite is estimated to occur for maximum cooling rates of ~5,000°C Ma⁻¹ at 320°C (Yang & Goldstein, 2004), while the cloudy zone microstructure forms at an estimated maximum cooling rate of ~10,000°C Ma⁻¹ at 350°C (Maurel et al., 2019). It is currently not clear if the uncertainties on these two critical cooling rates overlap. If they are not within error of each other, this would mean that any meteorite with a high-Ni taenite rim containing tetraenaite should also have formed a cloudy zone in this region. If a cloudy zone is in fact present in Acapulco, then the maximum cooling rate at 350°C is ~5,000°C Ma⁻¹. If no cloudy zone is present, then we would interpret this under the assumption that the two critical cooling rates have overlapping uncertainties, in which case Acapulco cooled <~10,000°C Ma⁻¹ at 320°C. In summary, our data indicate that Acapulco cooled slower than ~5,000–10,000°C Ma⁻¹ at 320–350°C, which is consistent with the reported metallographic cooling rates 10³–10⁵°C Ma⁻¹ at temperatures of 350–600°C for acapulcoites (Keil & McCoy, 2018), albeit on the lower end of that range.

Our reported cooling rate at 320–350°C has important implications for the thermal evolution of the AL parent body. ALs must have been part of a body at least 2 km in radius based on recent cooling rates reported for lodranites (Lucas et al., 2022). For such a 2 km radius body, ALs would have to be located within 10% of the radius of the center of the body. The depth of emplacement within the body decreases as the size of the body increases. Therefore, either the AL parent body was never disrupted prior to cooling through 320°C and instead underwent monotonic cooling through this temperature, or the body was disrupted above this temperature and ALs were later reaccreted into a secondary body of at least a few km in radius. The low-temperature cooling rate constraint imposed by tetraenaite suggests it is highly unlikely that the AL parent body was catastrophically disrupted and did not undergo at least partial recreation.

The presence of two ferromagnetic minerals in Acapulco that would have acquired their NRMs at different times enables the possibility of further constraining the thermal evolution of the parent body under the assumption that the two minerals acquire magnetizations independently of each other. Recent discussion of the potential inheritance of NRM during pseudomorphic replacement of FeNi metal to magnetite (Borlina et al., 2022; Bryson et al., 2023) suggests that the influence of kamacite on neighboring taenite and the inheritance of tetrataenite magnetization from the precursor taenite should be studied further. Here, we present the methods by which a future paleomagnetic study of Acapulco or other members of the AL clan could elucidate the structure and history of the body. We consider that the parent body experienced one of four evolutionary paths (Figure 9) after initial heating of the ALSR source region [outer 7–25 km (Neumann et al., 2018)] (ALSR), to peak temperatures of 1,200°C [note that the deeper interior could have reached 1,625°C as suggested by three-dimensional thermal modeling of the parent body (Neumann et al., 2018)]: 1) Continuous cooling without major disruption by impacts; 2) Catastrophic disruption at the time that the ALSR reached its peak temperature followed by re-accretion and final cooling; 3) Catastrophic disruption when the temperature of the ALSR \sim 500°C and then re-accretion and final cooling; 4) Catastrophic disruption at the time that the ALSR reached its peak temperature followed by no reaccrction.

In each path, we start with the ALSR having reached its peak temperature and possessing an onion-shell structure as suggested by previous thermal models (Golabek et al., 2014; Neumann et al., 2018; Touboul et al., 2009). We allow for a chondritic crust to overlay a primitive achondritic layer that in turn overlies an igneous silicate region and possibly also a metallic core. In Case 1A, we consider a parent body evolution model in which the body possessed a tens of km radius metallic core that was capable of generating a dynamo (Bryson et al., 2019; Dodds et al., 2021; Weiss et al., 2010) on the tens-hundreds of Ma timescale like that found for IIIe irons (Maurel et al., 2020, 2021). In this scenario, the ALSR cools continuously from peak temperatures down to below 320°C. If the dynamo was present continuously, then both kamacite and tetrataenite in Acapulco would have acquired a NRM record of the dynamo during cooling through their blocking and ordering temperatures of 780°C (or lower as suggested by subsolidus recrystallization) and 320°C, respectively. However, the external field direction and strength may have changed between the times at which the NRMs were acquired by the two minerals or even changed while each mineral acquired its NRM.

In Case 1B, we consider the scenario in which the parent body continuously cooled, but there was either no core present or a core was present but was not able to generate a dynamo field. In this case, the parent body cools through the ordering and blocking temperatures of tetrataenite and kamacite but there is no external field recorded. In Case 2, the parent body was disrupted around ALSR peak temperatures and then reaccrcted as solid fragments prior to ALSR cooling to 750°C [following (15)]. We expect that it is unlikely that a molten core formed that was sufficiently large to be able to generate a dynamo on the secondary body. Therefore, in both Cases 1B and 2, kamacite and tetrataenite would not have recorded a dynamo field.

In Case 3, the parent body was disrupted at a temperature after the ALSR cooled to below the blocking temperature of kamacite. In Case 3A, the parent body possessed a dynamo and the ALSR cooled through 780°C, which would enable the kamacite to retain a record of the external field. However, the body was then disrupted at ALSR temperatures \sim 500°C [as suggested by ref. (Göpel & Manhès, 2010)], and subsequently reaccrcted. As before, it is highly unlikely that there would have been an advecting metal core capable of creating a dynamo field after reaccrction, and therefore the tetrataenite would not have recorded any field when the ALSR reached 320°C. However, as noted previously, this assumes that the remanence of kamacite has no effect on the magnetization of the tetrataenite. Case 3B describes the evolution of a body that had no dynamo prior to disruption and therefore no dynamo field was recorded by the kamacite or tetrataenite.

In Case 4, the parent body is catastrophically disrupted into pieces <2 km in radius at ALSR peak temperatures and never reaccrcted. As discussed previously, this path is not likely as ALs must have cooled at rates $<\sim$ 5,000–10,000°C Ma⁻¹ at 320–350°C.

In summary, a thorough understanding of the paleomagnetic record of the tetrataenite and kamacite separately in ALs may distinguish between different parent body evolution paths. In the case where no field is recorded by either kamacite or tetrataenite, we would be unable to differentiate between Cases 1B, 2, or 3B. However, if both tetrataenite and kamacite show evidence for a dynamo field being present at their respective NRM acquisition temperatures, then the parent body was not likely disrupted and followed the path described in

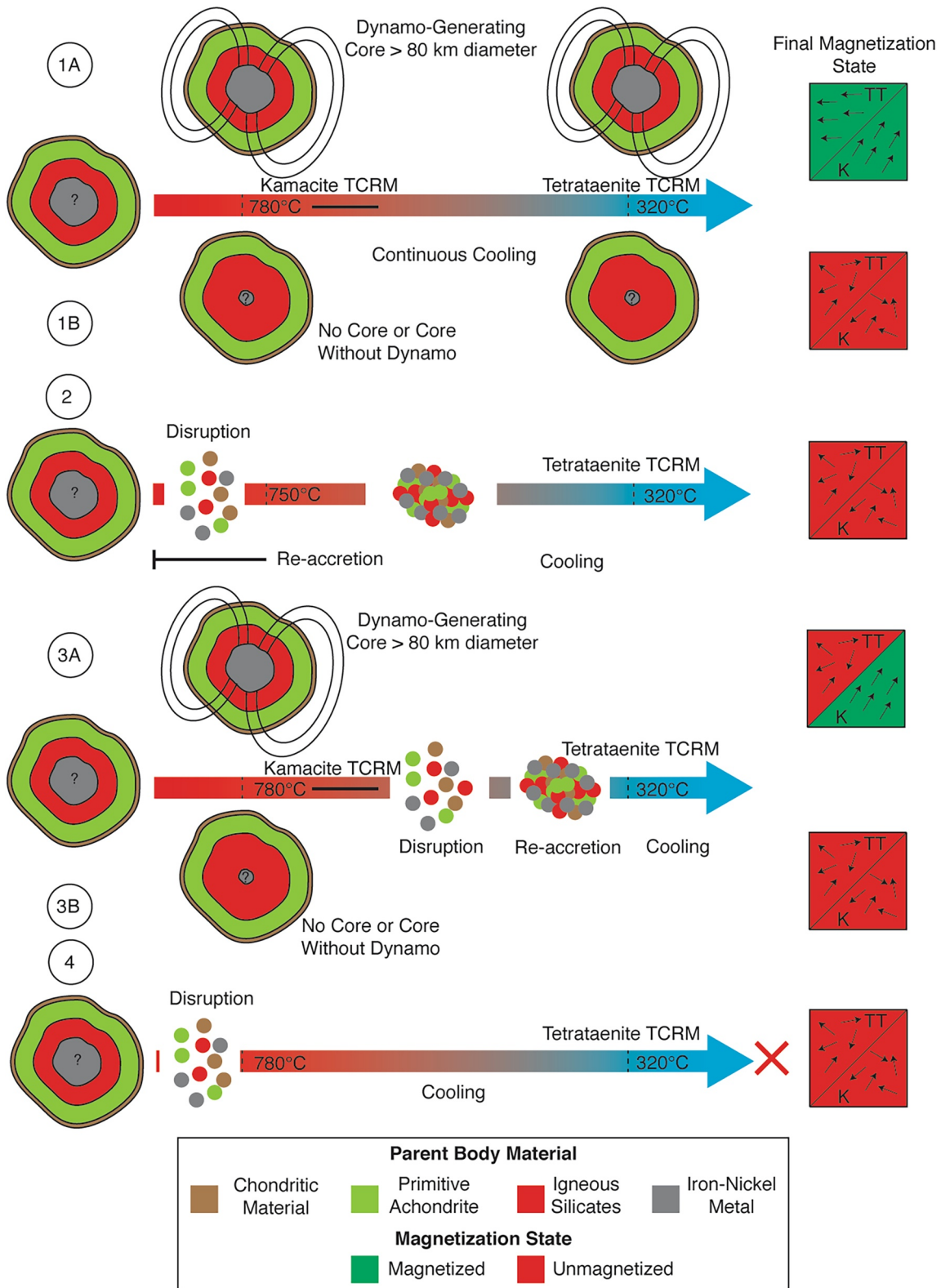


Figure 9.

Case 1A. In this scenario, one potential explanation for the varying cooling rates reported for ALs could be impact unroofing of the material overlaying the ALs. Lastly, if kamacite contains an NRM record of a dynamo, but tetraenaite does not, then this would be consistent with catastrophic disruption below 780°C (i.e., Case 3A). However, an alternate explanation is that the dynamo ceased prior to reaching 320°C on a non-disrupted parent body.

Given the uniquely powerful ability of paleomagnetism to independently confirm the presence or absence of a dynamo on the AL parent body and therefore a metallic core larger than ~80 km in diameter (Weiss et al., 2010), further evaluation of the paleomagnetic record of ALs could provide valuable information to distinguish between the four abovementioned scenarios. Future paleomagnetic studies should focus on MBSs as they contain magnetic recorders that are more likely to be SD or SV compared to the bulk samples. However, an additional understanding of the acquisition of TCRMs by kamacite and tetraenaite is warranted prior to re-evaluating the paleomagnetic record of Acapulco. Alternately, future identification with transmission electron microscopy of a cloudy zone microstructure in Acapulco could enable a paleomagnetic study using X-ray photoemission electron microscopy (Bryson et al., 2014). An additional option for AL paleomagnetic studies is to focus on those ALs with MBSs that cooled at rates >5,000 to 10,000°C Ma⁻¹ and therefore would not possess tetraenaite. As an example, the Monument Draw acapulcoite has a reported metallographic cooling rate of ~10⁴°C Ma⁻¹ over the temperature range 600–350°C (McCoy et al., 1996). No lodranites have reported cooling rates around 320°C that are above 10⁴°C Ma⁻¹ (Keil & McCoy, 2018). However, an alternative path is to identify very slowly cooled lodranites (<10³°C Ma⁻¹) and search for cloudy zones as well.

5. Conclusions

- We present the results of a rock magnetic study of Acapulco and provide the initial results of the first paleomagnetic study of a primitive achondrite to determine if the parent body possessed a planetesimal dynamo.
- The major magnetic phases in bulk Acapulco samples are multidomain kamacite and tetraenaite, though there may be SD tetraenaite present in the plessite.
- The major magnetic phases in MBSs are kamacite and tetraenaite as well, but with smaller, potentially SD or SV grains sizes.
- Acapulco shows no evidence of remagnetization from a magnet or terrestrial weathering and therefore can retain a pre-terrestrial magnetic record.
- Bulk samples are poor recorders due to large interstitial metal grains that dominate the measured NRM magnetization.
- The NRM magnetizations in MBSs are summations of multiple ferromagnetic minerals that would have acquired magnetizations at different times and in different forms, leading to complex NRMs that do not allow us to definitely conclude that a dynamo was present or absent on the parent body.
- No primary NRM components were isolated during AF demagnetization of MBS.
- The presence of tetraenaite indicates that Acapulco underwent slow cooling (<~5,000–10,000°C Ma⁻¹) at 320–350°C. This suggests that it is highly unlikely that the parent body was catastrophically disrupted while Acapulco was at peak temperatures without subsequent reaccretion.
- Future paleomagnetic investigations of Acapulco that can interpret the magnetization of kamacite and tetraenaite separately may be able to determine the evolution of the parent body.

Figure 9. Parent body evolution scenarios. In Case 1, the parent body cooled without being disrupted and possessed (Case 1A) or lacked (Case 1B) a dynamo. We note that the direction of the cartoon magnetization is chosen to be arbitrary. In Case 2, the parent body was disrupted by impacts at peak temperatures and subsequently reaccreted to form a secondary body of at least 2 km in radius. No dynamo ever formed in this scenario. In Case 3, the parent body began to cool but was later disrupted and reaccreted. If a dynamo was present prior to disruption (Case 3A), then the kamacite would have acquired NRM in the field. In Case 4, the parent body was catastrophically disrupted at peak temperatures and never reaccreted. The cooling rate threshold imposed by the presence of tetraenaite excludes Case 4 for the AL parent body (as denoted by “X”). The final magnetization states of the kamacite and tetraenaite for each Case are shown to the right. *K* = kamacite, *T* = tetraenaite.

Data Availability Statement

Magnetization files that contain data on the NRM demagnetization of all bulk samples and their magnetic properties used to draw the conclusions in this paper can be found on the Magnetism Information Consortium (MagIC) database via <https://doi.org/10.7288/V4/MAGIC/19872> (Mansbach et al., 2023) as a zip file. The MagIC database DOI also contains .mat files with all SQUID maps taken of MBS magnetizations including NRM demagnetization, thermal demagnetization, ARM demagnetization, and IRM demagnetization.

Acknowledgments

We acknowledge funding from NASA FINESST Grant 80NSSC20K1366 and a private gift from Thomas F. Peterson, Jr. We thank Tim Grove for productive conversations about primitive chondrites and planetary differentiation and Caroline Ross for the use of her vibrating sample magnetometer. We also thank Tim McCoy and the Smithsonian Institute staff for providing meteorite samples for this study. Lastly, we thank Wyn Williams and Richard Harrison for insightful and constructive reviews to improve the manuscript.

References

- Benedix, G. K., & Lauretta, D. S. (2006). Thermodynamic constraints on the formation history of acapulcoites. *Lunar and Planetary Science Conference*, 37, 2129.
- Bezaeva, N. S., Gattacceca, J., Rochette, P., & Sadykov, R. A. (2022). Demagnetization of ordinary chondrites under hydrostatic pressure up to 1.8 GPa. *Geochemistry International*, 60(5), 421–429. <https://doi.org/10.1134/s0016702922050032>
- Bild, R. W., & Wasson, J. T. (1976). The Lodran meteorite and its relationship to the ureilites. *Mineralogical Magazine*, 40(315), 721–735. <https://doi.org/10.1180/minmag.1976.040.315.06>
- Blukis, R., Pfau, B., Günther, C. M., Hessing, P., Eisebitt, S., Einsle, J., & Harrison, R. J. (2020). Nanoscale imaging of high-field magnetic hysteresis in meteoritic metal using X-ray holography. *Geochemistry, Geophysics, Geosystems*, 21(8), e2020GC009044. <https://doi.org/10.1029/2020gc009044>
- Borlina, C. S., Weiss, B. P., Bryson, J. F. J., & Armitage, P. J. (2022). Lifetime of the outer solar system nebula from carbonaceous chondrites. *Journal of Geophysical Research: Planets*, 127(7), e2021JE007139. <https://doi.org/10.1029/2021je007139>
- Borlina, C. S., Weiss, B. P., Bryson, J. F. J., Bai, X., Lima, E. A., Chatterjee, N., & Mansbach, E. N. (2021). Paleomagnetic evidence for a disk substructure in the early solar system. *Science Advances*, 7(42), eabj6928. <https://doi.org/10.1126/sciadv.abj6928>
- Bryson, J. F. J., Herrero-Albillos, J., Kronast, F., Ghidini, M., Redfern, S. A. T., van der Laan, G., & Harrison, R. J. (2014). Nanopaleomagnetism of meteoritic Fe–Ni studied using X-ray photoemission electron microscopy. *Earth and Planetary Science Letters*, 396, 125–133. <https://doi.org/10.1016/j.epsl.2014.04.016>
- Bryson, J. F. J., Neufeld, J. A., & Nimmo, F. (2019). Constraints on asteroid magnetic field evolution and the radii of meteorite parent bodies from thermal modelling. *Earth and Planetary Science Letters*, 521, 68–78. <https://doi.org/10.1016/j.epsl.2019.05.046>
- Bryson, J. F. J., Nichols, C. I. O., & Mac Niocaill, C. (2023). A unified intensity of the magnetic field in the protoplanetary disk from the Winchcombe meteorite. *Meteoritics & Planetary Sciences*. <https://doi.org/10.1111/maps.14079>
- Dhaliwal, J. K., Day, J. M. D., Corder, C. A., Tait, K. T., Marti, K., Assayag, N., et al. (2017). Early metal-silicate differentiation during planetesimal formation revealed by acapulcoite and lodranite meteorites. *Geochimica et Cosmochimica Acta*, 216, 115–140. <https://doi.org/10.1016/j.gca.2017.06.042>
- Dodds, K. H., Bryson, J. F. J., Neufeld, J. A., & Harrison, R. J. (2021). The thermal evolution of planetesimals during accretion and differentiation: Consequences for dynamo generation by thermally-driven convection. *Journal of Geophysical Research: Planets*, 126(3). <https://doi.org/10.1029/2020je006704>
- Dos Santos, E., Gattacceca, J., Rochette, P., Fillion, G., & Scorzelli, R. B. (2015). Kinetics of tetraenaite disordering. *Journal of Magnetism and Magnetic Materials*, 375, 234–241. <https://doi.org/10.1016/j.jmmm.2014.09.051>
- Dunlop, D. J., & Argyle, K. S. (1997). Thermoremanence, anhysteretic remanence and susceptibility of submicron magnetites: Nonlinear field dependence and variation with grain size. *Journal of Geophysical Research*, 102(B9), 20199–20210. <https://doi.org/10.1029/97jb00957>
- Einsle, J. F., Eggeman, A. S., Martineau, B. H., Saghi, Z., Collins, S. M., Blukis, R., et al. (2018). Nanomagnetic properties of the meteorite cloudy zone. *Proceedings of the National Academy of Sciences of the United States of America*, 115(49), E11436–E11445. <https://doi.org/10.1073/pnas.1809378115>
- El Goresy, A., Zinner, E., Pellas, P., & Caillet, C. (2005). A menagerie of graphite morphologies in the Acapulco meteorite with diverse carbon and nitrogen isotopic signatures: Implications for the evolution history of acapulcoite meteorites. *Geochimica et Cosmochimica Acta*, 69(18), 4535–4556. <https://doi.org/10.1016/j.gca.2005.03.051>
- Fu, R. R., Lima, E. A., Volk, M. W. R., & Trubko, R. (2020). High-sensitivity moment magnetometry with the quantum diamond microscope. *Geochemistry, Geophysics, Geosystems*, 21(8), e2020GC009147. <https://doi.org/10.1029/2020gc009147>
- Fu, R. R., Weiss, B. P., Lima, E. A., Harrison, R. J., Bai, X.-N., Desch, S. J., et al. (2014). Solar nebula magnetic fields recorded in the Semarkona meteorite. *Science*, 346(6213), 1089–1092. <https://doi.org/10.1126/science.1258022>
- Garrick-Bethell, I., & Weiss, B. P. (2010). Kamacite blocking temperatures and applications to lunar magnetism. *Earth and Planetary Science Letters*, 294(1), 1–7. <https://doi.org/10.1016/j.epsl.2010.02.013>
- Garrick-Bethell, I., Weiss, B. P., Shuster, D. L., & Buz, J. (2009). Early lunar magnetism. *Science*, 323(5912), 356–359. <https://doi.org/10.1126/science.1166804>
- Gattacceca, J., Boustie, M., Hood, L., Cuq-Lelandais, J. P., Fuller, M., Bezaeva, N. S., et al. (2010). Can the lunar crust be magnetized by shock? Experimental groundtruth. *Earth and Planetary Science Letters*, 299(1–2), 42–53. <https://doi.org/10.1016/j.epsl.2010.08.011>
- Gattacceca, J., & Rochette, P. (2004). Toward a robust normalized magnetic paleointensity method applied to meteorites. *Earth and Planetary Science Letters*, 227(3–4), 377–393. <https://doi.org/10.1016/j.epsl.2004.09.013>
- Gattacceca, J., Suavet, C., Rochette, P., Weiss, B. P., Winkhofer, M., Uehara, M., & Friedrich, J. M. (2014). Metal phases in ordinary chondrites: Magnetic hysteresis properties and implications for thermal history. *Meteoritics & Planetary Sciences*, 49(4), 652–676. <https://doi.org/10.1111/maps.12268>
- Glenn, D. R., Fu, R. R., Kehayias, P., Sage, D. L., Lima, E. A., Weiss, B. P., & Walsworth, R. L. (2017). Micrometer-scale magnetic imaging of geological samples using a quantum diamond microscope. *Geochemistry, Geophysics, Geosystems*, 18(8), 3254–3267. <https://doi.org/10.1002/2017gc006946>
- Golabek, G. J., Bourdon, B., & Gerya, T. V. (2014). Numerical models of the thermomechanical evolution of planetesimals: Application to the acapulcoite-lodranite parent body. *Meteoritics & Planetary Sciences*, 49(6), 1083–1099. <https://doi.org/10.1111/maps.12302>
- Goldstein, J. I., & Michael, J. R. (2006). The formation of plessite in meteoritic metal. *Meteoritics & Planetary Sciences*, 41(4), 553–570. <https://doi.org/10.1111/j.1945-5100.2006.tb00482.x>
- Göpel, C., & Manhès, G. (2010). The thermal history of the Acapulco meteorite and its parent body deduced from U/Pb systematics in mineral separates and bulk rock fragments. *Comptes Rendus Geoscience*, 342(1), 53–59. <https://doi.org/10.1016/j.crte.2009.10.013>

- Greenwood, R. C., Burbine, T. H., Miller, M. F., & Franchi, I. A. (2017). Melting and differentiation of early-formed asteroids: The perspective from high precision oxygen isotope studies. *Geochemistry*, 77(1), 1–43. <https://doi.org/10.1016/j.chemer.2016.09.005>
- Greenwood, R. C., Franchi, I. A., Gibson, J. M., & Benedix, G. K. (2012). Oxygen isotope variation in primitive achondrites: The influence of primordial, asteroidal and terrestrial processes. *Geochimica et Cosmochimica Acta*, 94, 146–163. <https://doi.org/10.1016/j.gca.2012.06.025>
- Harrison, R. J., & Feinberg, J. M. (2008). FORCinel: An improved algorithm for calculating first-order reversal curve distributions using locally weighted regression smoothing. *Geochemistry, Geophysics, Geosystems*, 9(5). <https://doi.org/10.1029/2008gc001987>
- Keil, K., & McCoy, T. J. (2018). Acapulcoite-lodranite meteorites: Ultramafic asteroidal partial melt residues. *Geochemistry*, 78(2), 153–203. <https://doi.org/10.1016/j.chemer.2017.04.004>
- Khokhlov, A., & Hulot, G. (2015). Principal component analysis of palaeomagnetic directions: Converting a maximum angular deviation (MAD) into an α_{95} angle. *Geophysical Journal International*, 204(1), 274–291. <https://doi.org/10.1093/gji/ggv451>
- Kirschvink, J. L. (1980). The least-squares line and plane and the analysis of palaeomagnetic data. *Geophysical Journal International*, 62(3), 699–718. <https://doi.org/10.1111/j.1365-246x.1980.tb02601.x>
- Lappe, S. L. L., Church, N. S., Kasama, T., da Silva Fanta, A. B., Bromiley, G., Dunin-Borkowski, R. E., et al. (2011). Mineral magnetism of dusty olivine: A credible recorder of pre-accretionary remanence. *Geochemistry, Geophysics, Geosystems*, 12(12), Q12Z35. <https://doi.org/10.1029/2011gc003811>
- Lappe, S. L. L., Feinberg, J. M., Muxworthy, A. R., & Harrison, R. J. (2013). Comparison and calibration of nonheating paleointensity methods: A case study using dusty olivine. *Geochemistry, Geophysics, Geosystems*, 14(7), 2143–2158. <https://doi.org/10.1002/ggge.20141>
- Lima, E. A., & Weiss, B. P. (2016). Ultra-high sensitivity moment magnetometry of geological samples using magnetic microscopy. *Geochemistry, Geophysics, Geosystems*, 17(9), 3754–3774. <https://doi.org/10.1002/2016gc006487>
- Lucas, M. P., Dygert, N., Ren, J., Hesse, M. A., Miller, N. R., & McSween, H. Y. (2022). Thermochemical evolution of the acapulcoite-lodranite parent body: Evidence for fragmentation-disrupted partial differentiation. *Meteoritics & Planetary Sciences*, 57(12), 2248–2275. <https://doi.org/10.1111/maps.13930>
- Mansbach, E. N., Shah, J., Williams, W., Maurel, C., Bryson, J. F. J., & Weiss, B. P. (2022). Size ranges of magnetic domain states in tetraenaite. *Geochemistry, Geophysics, Geosystems*, 23(11). <https://doi.org/10.1029/2022gc010631>
- Mansbach, E. N., Weiss, B. P., Schnepf, N. R., Lima, E. A., Borlina, C. S., Chatterjee, N., et al. (2023). Magnetism of the acapulco primitive achondrite and implications for the evolution of partially differentiated bodies. *Magnetics Information Consortium (MagIC)*. <https://doi.org/10.7288/V4/MAGIC/19872>
- Maurel, C., Bryson, J. F. J., Lyons, R. J., Ball, M. R., Chopdekar, R. V., Scholl, A., et al. (2020). Meteorite evidence for partial differentiation and protracted accretion of planetesimals. *Science Advances*, 6(30), eaba1303. <https://doi.org/10.1126/sciadv.aba1303>
- Maurel, C., Bryson, J. F. J., Shah, J., Chopdekar, R. V., T. Elkins-Tanton, L., A. Raymond, C., & Weiss, B. P. (2021). A long-lived planetesimal dynamo powered by core crystallization. *Geophysical Research Letters*, 48(6), e2020GL091917. <https://doi.org/10.1029/2020gl091917>
- Maurel, C., Weiss, B. P., & Bryson, J. F. J. (2019). Meteorite cloudy zone formation as a quantitative indicator of paleomagnetic field intensities and cooling rates on planetesimals. *Earth and Planetary Science Letters*, 513, 166–175. <https://doi.org/10.1016/j.epsl.2019.02.027>
- McClelland, E. (1996). Theory of CRM acquired by grain growth, and its implications for TRM discrimination and paleointensity determination in igneous rocks. *Geophysical Journal International*, 126(1), 271–280. <https://doi.org/10.1111/j.1365-246x.1996.tb05285.x>
- McCoy, T. J., Keil, K., Clayton, R. N., Mayeda, T. K., Bogard, D. D., Garrison, D. H., et al. (1996). A petrologic, chemical, and isotopic study of meteorite draw and comparison with other acapulcoites: Evidence for formation by incipient partial melting. *Geochimica et Cosmochimica Acta*, 60(14), 2681–2708. [https://doi.org/10.1016/0016-7037\(96\)00109-3](https://doi.org/10.1016/0016-7037(96)00109-3)
- McCoy, T. J., Keil, K., Muenow, D. W., & Wilson, L. (1997). Partial melting and melt migration in the acapulcoite-lodranite parent body. *Geochimica et Cosmochimica Acta*, 61(3), 639–650. [https://doi.org/10.1016/s0016-7037\(96\)00365-1](https://doi.org/10.1016/s0016-7037(96)00365-1)
- Muxworthy, A. R., & Roberts, A. P. (2007). First-order reversal curve (FORC) diagrams. In D. Gubbins & E. Herrero-Bervera (Eds.), *Encyclopedia of geomagnetism and paleomagnetism* (pp. 266–272). Springer Netherlands.
- Neumann, W., Henke, S., Breuer, D., Gail, H., Schwarz, W. H., Trieloff, M., et al. (2018). Modeling the evolution of the parent body of acapulcoites and lodranites: A case study for partially differentiated asteroids. *Icarus*, 311, 146–169. <https://doi.org/10.1016/j.icarus.2018.03.024>
- Nichols, C. I. O., Bryson, J. F. J., Blukis, R., Herrero-Albillos, J., Kronast, F., Rüffer, R., et al. (2020). Variations in the magnetic properties of meteoritic cloudy zone. *Geochemistry, Geophysics, Geosystems*, 21(2), e2019GC008798. <https://doi.org/10.1029/2019gc008798>
- Nichols, C. I. O., Krakow, R., Herrero-Albillos, J., Kronast, F., Northwood-Smith, G., & Harrison, R. J. (2018). Microstructural and paleomagnetic insight into the cooling history of the IAB parent body. *Geochimica et Cosmochimica Acta*, 229, 1–19. <https://doi.org/10.1016/j.gca.2018.03.009>
- Ohtani, E., Sakurabayashi, T., & Kurosawa, K. (2022). Experimental simulations of shock textures in bcc iron: Implications for iron meteorites. *Progress in Earth and Planetary Science*, 9(1), 24. <https://doi.org/10.1186/s40645-022-00482-7>
- Palme, H., Schultz, L., Spettel, B., Weber, H. W., Wänke, H., Michel-Levy, M. C., & Lorin, J. C. (1981). The Acapulco meteorite: Chemistry, mineralogy and irradiation effects. *Geochimica et Cosmochimica Acta*, 45(5), 727–752. [https://doi.org/10.1016/0016-7037\(81\)90045-4](https://doi.org/10.1016/0016-7037(81)90045-4)
- Renne, P. R. (2000). $^{40}\text{Ar}/^{39}\text{Ar}$ age of plagioclase from Acapulco meteorite and the problem of systematic errors in cosmochronology. *Earth and Planetary Science Letters*, 175(1–2), 13–26. [https://doi.org/10.1016/s0012-821x\(99\)00287-3](https://doi.org/10.1016/s0012-821x(99)00287-3)
- Rochette, P., Gattacceca, J., Bourot-Denise, M., Consolmagno, G., Folco, L., Kohout, T., et al. (2009). Magnetic classification of stony meteorites: 3. Achondrites. *Meteoritics & Planetary Sciences*, 44(3), 405–427. <https://doi.org/10.1111/j.1945-5100.2009.tb00741.x>
- Shah, J., Williams, W., Almeida, T. P., Nagy, L., Muxworthy, A. R., Kovács, A., et al. (2018). The oldest magnetic record in our solar system identified using nanometric imaging and numerical modeling. *Nature Communications*, 9(1), 1173. <https://doi.org/10.1038/s41467-018-03613-1>
- Stephenson, A. (1993). Three-axis static alternating field demagnetization of rocks and the identification of natural remanent magnetization, gyromagnetic magnetization, and anisotropy. *Journal of Geophysical Research*, 98(B1), 373–381. <https://doi.org/10.1029/92jb01849>
- Suavet, C., Weiss, B. P., & Grove, T. L. (2014). Controlled-atmosphere thermal demagnetization and paleointensity analyses of extraterrestrial rocks. *Geochemistry, Geophysics, Geosystems*, 15(7), 2733–2743. <https://doi.org/10.1002/2013gc005215>
- Swartzendruber, L. J., Itkin, V. P., & Alcock, C. B. (1991). The Fe-Ni (iron-nickel) system. *Journal of Phase Equilibria*, 12(3), 288–312. <https://doi.org/10.1007/bf02649918>
- Tauxe, L. (2010). *Essentials of paleomagnetism*. University of California Press.
- Tauxe, L., & Staudigel, H. (2004). Strength of the geomagnetic field in the Cretaceous normal superchron: New data from submarine basaltic glass of the Troodos ophiolite. *Geochemistry, Geophysics, Geosystems*, 5(2), Q02H06. <https://doi.org/10.1029/2003gc000635>
- Tikoo, S. M., Weiss, B. P., Buz, J., Lima, E. A., Shea, E. K., Melo, G., & Grove, T. L. (2012). Magnetic fidelity of lunar samples and implications for an ancient core dynamo. *Earth and Planetary Science Letters*, 337–338, 93–103. <https://doi.org/10.1016/j.epsl.2012.05.024>

- Touboul, M., Kleine, T., Bourdon, B., Van Orman, J. A., Maden, C., & Zipfel, J. (2009). Hf–W thermochronometry: II. Accretion and thermal history of the acapulcoite–lodranite parent body. *Earth and Planetary Science Letters*, 284(1–2), 168–178. <https://doi.org/10.1016/j.epsl.2009.04.022>
- Uehara, M., Gattacceca, J., Rochette, P., Demory, F., & Valenzuela, E. M. (2012). Magnetic study of meteorites recovered in the atacama desert (Chile): Implications for meteorite paleomagnetism and the stability of hot desert surfaces. *Physics of the Earth and Planetary Interiors*, 200–201, 113–123. <https://doi.org/10.1016/j.pepi.2012.04.007>
- Vervelidou, F., Weiss, B. P., & Lacroix, F. (2023). Hand magnets and the destruction of ancient meteorite magnetism. *Journal of Geophysical Research: Planets*, 128(4), e2022JE007464. <https://doi.org/10.1029/2022je007464>
- Wang, H., Wang, J., Chen-Wiegart, Y. C., & Kent, D. V. (2015). Quantified abundance of magnetofossils at the Paleocene-Eocene boundary from synchrotron-based transmission X-ray microscopy. *Proceedings of the National Academy of Sciences of the United States of America*, 112(41), 12598–12603. <https://doi.org/10.1073/pnas.1517475112>
- Wang, H., Weiss, B. P., Bai, X. N., Downey, B. G., Wang, J., Wang, J., et al. (2017). Lifetime of the solar nebula constrained by meteorite paleomagnetism. *Science*, 355(6325), 623–627. <https://doi.org/10.1126/science.aaf5043>
- Weisberg, M. W., McCoy, T. J., & Krot, A. N. (2006). Systematics and evaluation of meteorite classification. In *Meteorites and the early solar system II*.
- Weiss, B. P., Berdahl, J. S., Elkins-Tanton, L., Stanley, S., Lima, E. A., & Carporzen, L. (2008). Magnetism on the angrite parent body and the early differentiation of planetesimals. *Science*, 322(5902), 713–716. <https://doi.org/10.1126/science.1162459>
- Weiss, B. P., & Elkins-Tanton, L. T. (2013). Differentiated planetesimals and the parent bodies of chondrites. *Annual Review of Earth and Planetary Sciences*, 41(1), 529–560. <https://doi.org/10.1146/annurev-earth-040610-133520>
- Weiss, B. P., Gattacceca, J., Stanley, S., Rochette, P., & Christensen, U. R. (2010). Paleomagnetic records of meteorites and early planetesimal differentiation. *Space Science Reviews*, 152(1–4), 341–390. <https://doi.org/10.1007/s11214-009-9580-z>
- Weiss, B. P., Lima, E. A., Fong, L. E., & Baudenbacher, F. J. (2007). Paleomagnetic analysis using SQUID microscopy. *Journal of Geophysical Research*, 112(B9). <https://doi.org/10.1029/2007jb004940>
- Yang, J., & Goldstein, J. I. (2004). Magnetic contribution to the interdiffusion coefficients in bcc (α) and fcc (γ) Fe–Ni alloys. *Metallurgical and Materials Transactions A*, 35(6), 1681–1690. <https://doi.org/10.1007/s11661-004-0077-9>
- Yang, J., & Goldstein, J. I. (2005). The formation of the Widmanstätten structure in meteorites. *Meteoritics & Planetary Sciences*, 40(2), 239–253. <https://doi.org/10.1111/j.1945-5100.2005.tb00378.x>
- Yang, J., Goldstein, J. I., & Scott, E. R. D. (2007). Iron meteorite evidence for early formation and catastrophic disruption of protoplanets. *Nature*, 446(7138), 888–891. <https://doi.org/10.1038/nature05735>
- Yu, Y., Tauxe, L., & Gee, J. S. (2007). A linear field dependence of thermoremanence in low magnetic fields. *Physics of the Earth and Planetary Interiors*, 162(3), 244–248. <https://doi.org/10.1016/j.pepi.2007.04.008>
- Zipfel, J., Palme, H., Kennedy, A. K., & Hutcheon, I. D. (1995). Chemical composition and origin of the Acapulco meteorite. *Geochimica et Cosmochimica Acta*, 59(17), 3607–3627. [https://doi.org/10.1016/0016-7037\(95\)00226-p](https://doi.org/10.1016/0016-7037(95)00226-p)

References From the Supporting Information

- Bland, P., Zolensky, M., Benedix, G., & Sephton, M. (2006). Weathering of chondritic meteorites. *Meteorites and the Early Solar System II*, 1, 853–867.
- Boland, J. N., & Duba, A. (1981). Solid-state reduction of iron in olivine-planetary and meteoritic evolution. *Nature*, 294(5837), 142–144. <https://doi.org/10.1038/294142a0>
- Dunlop, D., & Özdemir, Ö. (1997). *Rock magnetism: Fundamentals and Frontiers* (1 ed.). Cambridge University Press.
- Leroux, H., Libourel, G., Lemelle, L., & Guyot, F. (2003). Experimental study and REM characterization of dusty olivines in chondrites: Evidence for formation by in situ reduction. *Meteoritics & Planetary Sciences*, 38(1), 81–94. <https://doi.org/10.1111/j.1945-5100.2003.tb01047.x>
- Uehara, M., Beek, C. J., Gattacceca, J., Skidanov, V. A., & Quesnel, Y. (2010). Advances in magneto-optical imaging applied to rock magnetism and paleomagnetism. *Geochemistry, Geophysics, Geosystems*, 11(5). <https://doi.org/10.1029/2009gc002653>
- Williams, G. M., & Pavlovic, A. S. (1968). The magnetostriction behavior of iron single crystals. *Journal of Applied Physics*, 39(2), 571–572. <https://doi.org/10.1063/1.2163525>
- Werwiński, M., & Marciniak, W. (2017). Ab initio study of magnetocrystalline anisotropy, magnetostriction, and fermi surface of $L1_0\text{FeNi}$ (tetra-tenite). *Journal of Physics D: Applied Physics*, 50(49), 495008. <https://doi.org/10.1088/1361-6463/aa958a>